Supplementary Information

Methods.

^{1}H, ^{13}C, and ^{19}F NMR spectra were recorded on a Varian AS400 or Agilent DD2 500 MHz apparatus in deuterated solvents. Chemical shifts were reported as δ values (ppm) relative to the residual protic solvent. The number-average ($\bar{M}n$) and weigh taverage ($\bar{M}w$) molecular weights were determined by size exclusion chromatography (SEC) using a Malvern HT-GPC equipped with an RI detector. The flow rate was fixed at 0.75 mL/min using 1,2,4- trichlorobenzene (TCB) (with 0.0125% BHT w/v) as the eluent. The temperature of the system was set to 110 °C. All the samples were prepared at concentrations of nominally 0.50 mg/mL in TCB. The sample vials were held at 110 °C with stirring for 1 h for complete dissolution. The calibration method used to generate the reported data was the classical polystyrene method using polystyrene standards which were dissolved in TCB. UV−vis absorption spectra were taken using a Thermo Scientific Genesys 10S spectrophotometer using 1 cm path-length quartz cells. For solid-state measurements, polymer solution was spin-cast on glass plates. Optical bandgaps were calculated from the onset of the absorption band. Cyclic voltammograms were recorded on a Solartron 1287 potentiostat using platinum wires as working electrode and counter electrode at a scan rate of 50 mV/s. The reference electrode was Ag/Ag+ (0.01 M $AgNO_3$ in acetonitrile), and the electrolyte was a solution of 0.1 M tetrabutylammonium hexafluorophosphate (Bu_4NPF_6) in dry acetonitrile. In these conditions, the oxidation potential of ferrocene was 0.09 V versus Ag/Ag^+, whereas the oxidation potential of ferrocene was 0.41 V versus saturated calomel electrode (SCE). The HOMO and LUMO energy levels were determined from the oxidation and reduction onsets (where the current differs from the baseline) assuming that SCE electrode is −4.71 eV from vacuum, as reported in the literature.65 Thermogravimetric analysis (TGA) measurements were carried out with a Mettler Toledo TGA SDTA 851e apparatus at a heating rate of 10 °C/min under a nitrogen atmosphere. The temperature of degradation (T_d) corresponds to a 5% weight loss. Differential scanning calorimetry (DSC) analyses were performed on a PerkinElmer DSC-7 instrument calibrated with ultrapure indium at a scanning rate of 10 °C/min under a nitrogen flow. X-ray diffraction (XRD) was conducted on a Bruker D8 Discover powder diffractometer with a standard Bragg–Bretano geometry and a microfocus X-ray source (IuS) (Cu-K-alpha, λ = 0.15418 nm) was used to collect the XRD patterns of the polymer thin films on dodecyltrichlorosilane (DDTS)-modified SiO_2/Si substrates.

Materials.

2,3-Dibromothiophene and N-fluorobenzenesulfonimide (NFSI) were purchased from Combiblocks. NFSI was recrystallized in diethyl ether prior to use. *n*-Octyldimethylchlorosilane was purchased from Gelest Inc.

Polymers

Optimisation table

Entry	Poly.	Cat.	Ligand	base	solvent	conditions	Yield	Mn (g/mol)	Ip
1	P2	Herrmann's	P(*o*MeO-Ph)$_3$	Cs_2CO_3	Tol., 0.1M	120°C, 18h	87%	9727	1.71
2	P3	Herrmann's	P(*o*MeO-Ph)$_3$	Cs_2CO_3	Tol., 0.1M	120°C, 18h	88%	13142	1.65
3[a]	P2	Pd_2dba_3	P(*o*MeO-Ph)$_3$	Cs_2CO_3	Tol., 0.1M	120°C, 18h	-	-	-
4[a]	P2	$Pd(OAc)_2$	-	Cs_2CO_3	DMAc, 0.1M	120°C, 18h	75%	-	-
5	P2	$Pd(OAc)_2$	-	Cs_2CO_3	DMAc/Tol., 0.1M	120°C, 18h	74%	22888	1.47
6	P3	$Pd(OAc)_2$	-	Cs_2CO_3	DMAc/Tol., 0.1M	120°C, 18h	82%	21905	1.75

[a] only oligomerization occurs, no GPC was realised.

General DHAP procedure

Alkylated fDT-DPP (1 eq.), fluorinated comonomer (1 eq.), palladium acetate (2% mol), Cs2CO3 (3 eq.), and pivalic acid (1 eq.) were put in a microwave vial with a magnetic stirring bar. The vial was sealed with a cap and then purged with nitrogen 3 times. Degassed and anhydrous toluene was added (C = 0.2 mol/L), and the microwave vial was heated at 120 °C. After heating for 18 h, the mixture was diluted in $CHCl_3$, poured in methanol and the solid was recovered by filtration using a 0.45 µm nylon filter. The polymer was washed using a Soxhlet apparatus with methanol, acetone, hexanes and then chloroform. The chloroform fraction was reduced to 5−10 mL and then poured in methanol. The polymer was recovered by filtration over a 0.45 µm nylon filter and dry under vacuum.

Cyclic Voltammetry curves

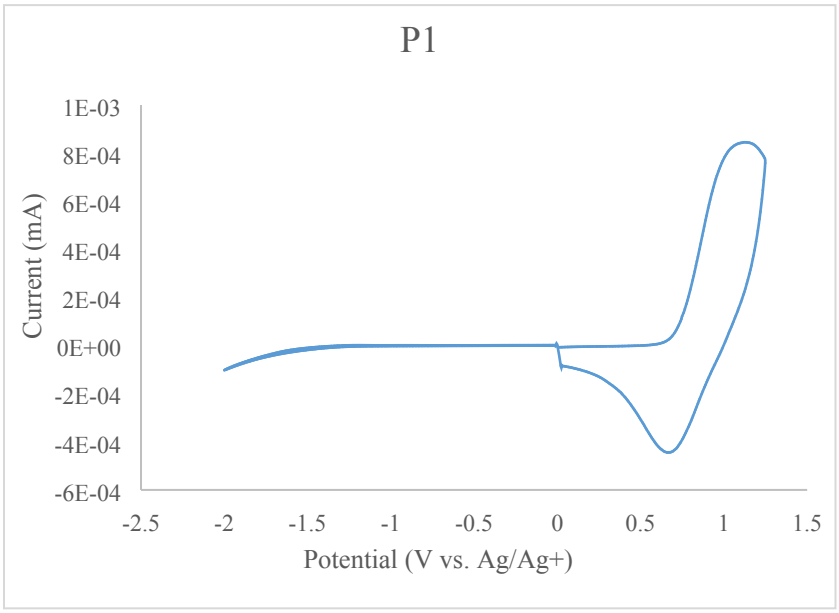

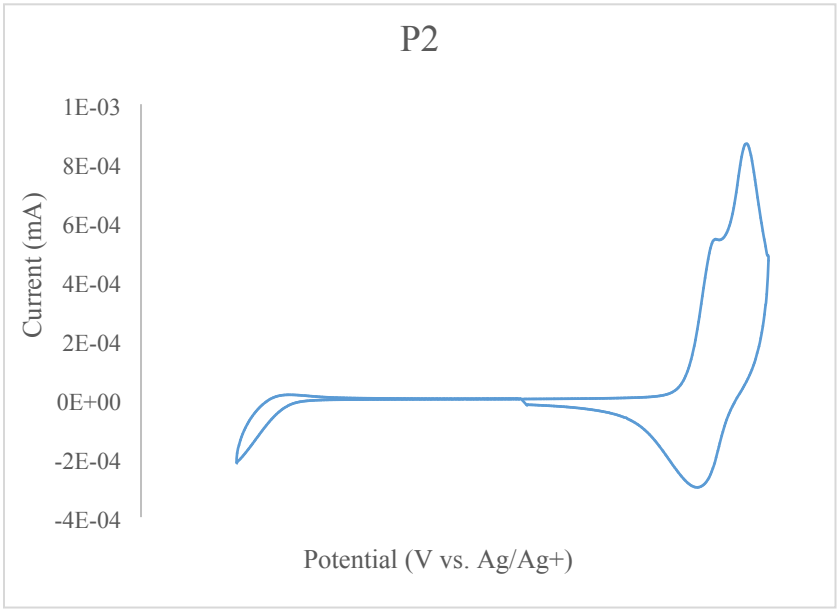

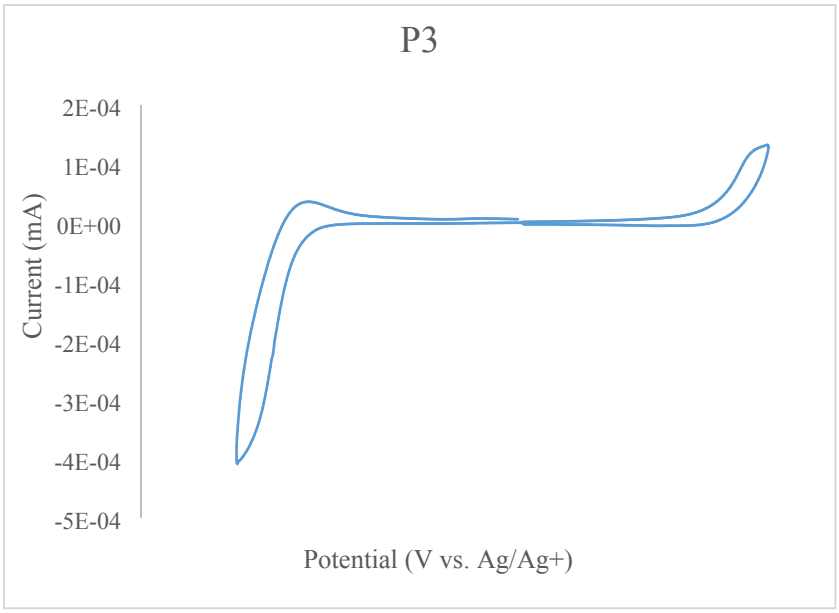
P3
2E-04
1E-04
0E+00
-1E-04
-2E-04
-3E-04
-4E-04
-5E-04
Current (mA)
Potential (V vs. Ag/Ag+)

TGA curves

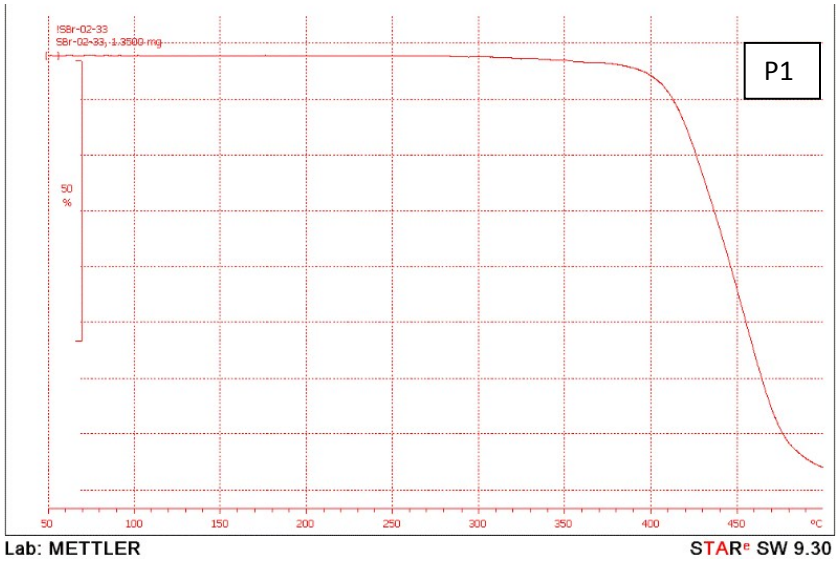
SBr-02-33
SBr-02-33, 1.3500 mg
P1
50
%
50
100
150
200
250
300
350
400
450
°C
Lab: METTLER
STARe SW 9.30

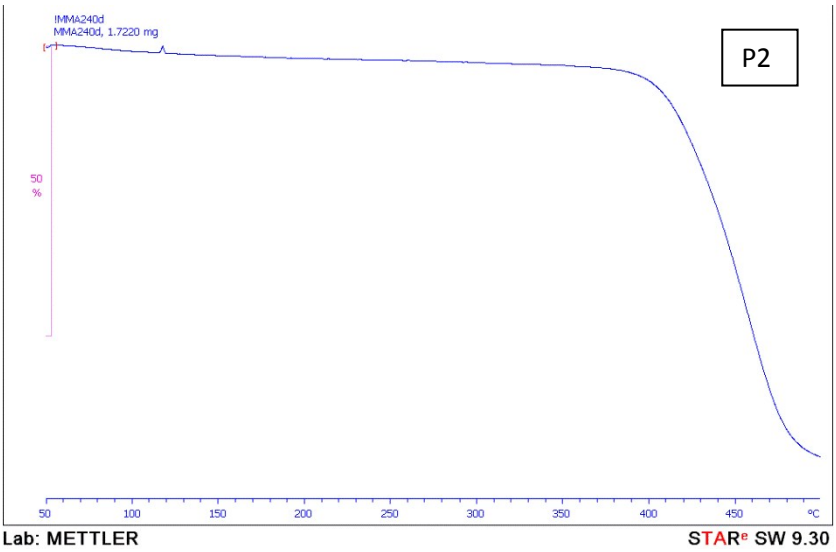

Lab: METTLER STARe SW 9.30

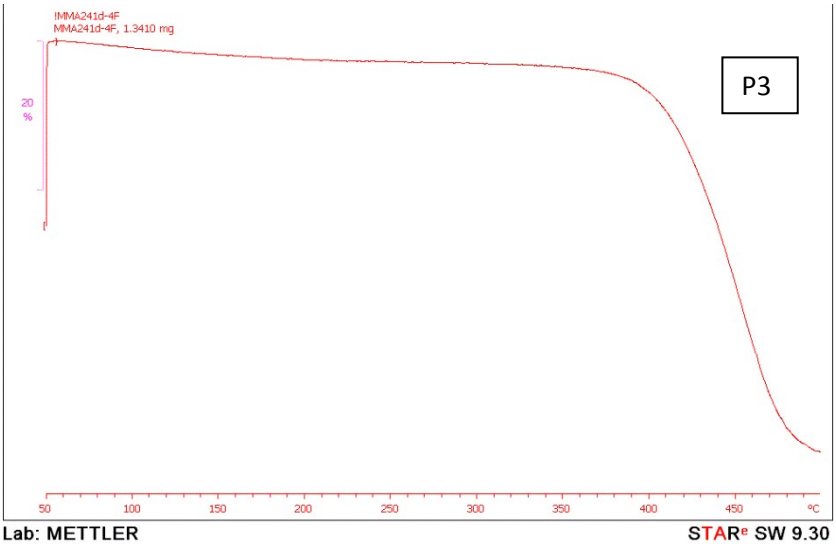

Lab: METTLER STARe SW 9.30

DSC curves

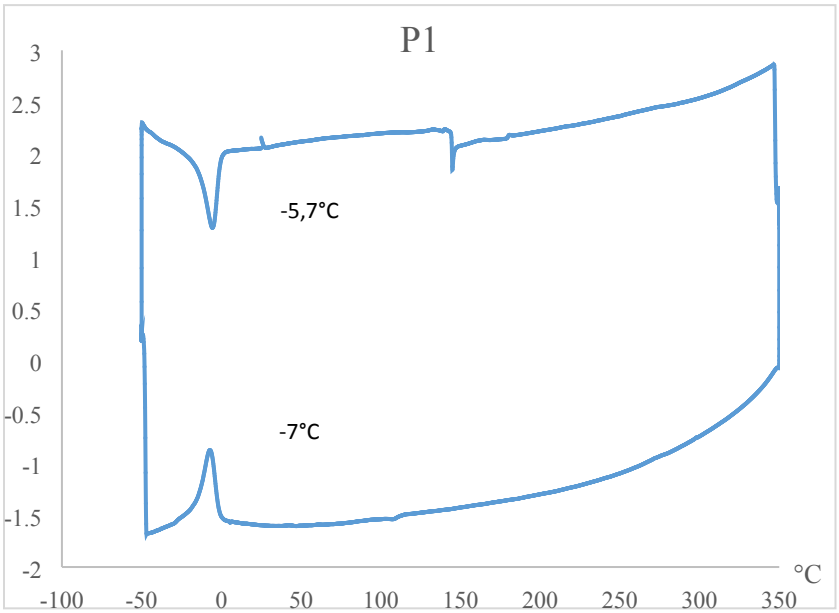
P1
3
2.5
2
1.5
1
0.5
0
-0.5
-1
-1.5
-2
-100
-50
0
50
100
150
200
250
300
350
°C
-5,7°C
-7°C

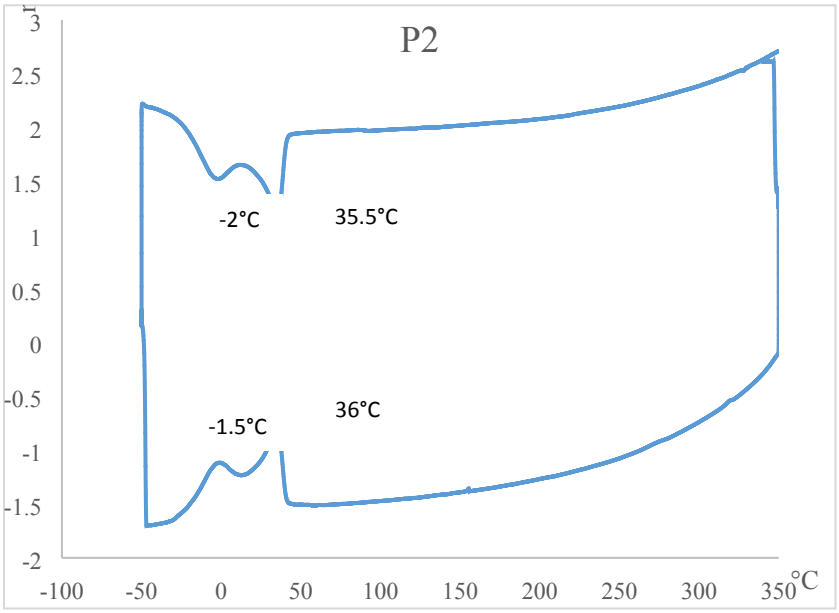
P2
3
2.5
2
1.5
1
0.5
0
-0.5
-1
-1.5
-2
-100
-50
0
50
100
150
200
250
300
350
°C
-2°C
35.5°C
-1.5°C
36°C

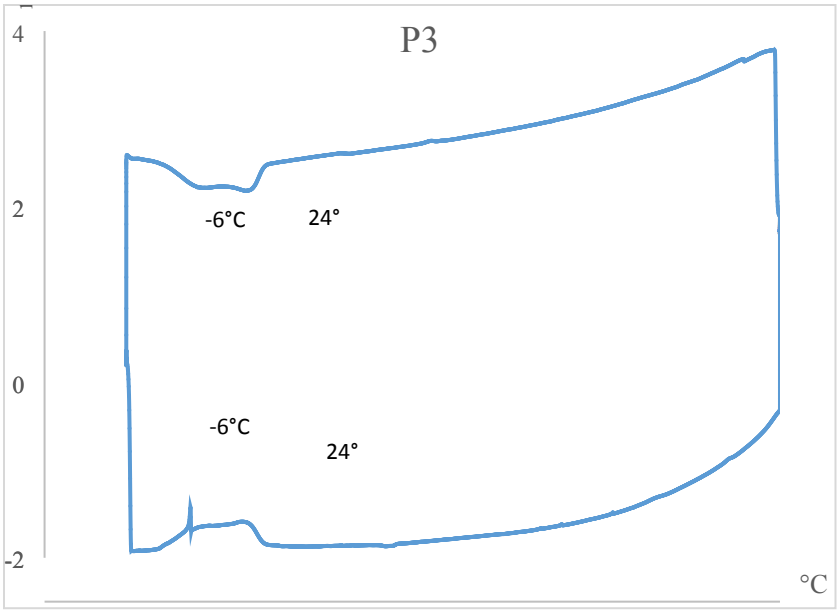
P3
4
2
0
-2
-6°C
24°
-6°C
24°
°C

DFT calculation

Density-functional theory (DFT) and time-dependent DFT (TDDFT) calculations were realized with wB97XD functional[1] and the 6-31+G(d,p) basis set as implemented by Gaussian 16, version.C.01. software package[2].

fDT-DPP-2F2Th

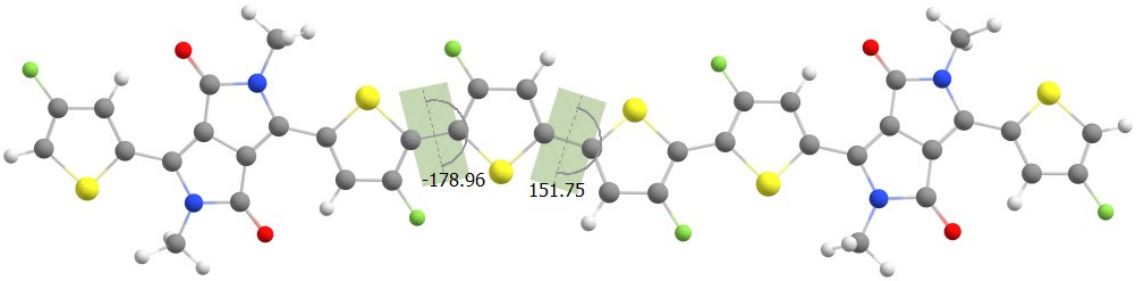

HOMO

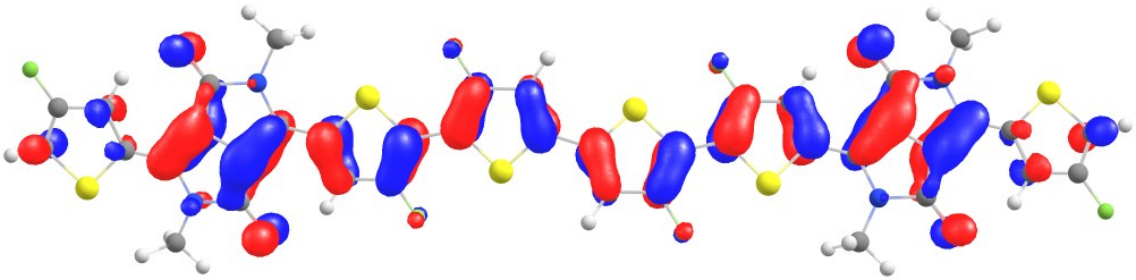

LUMO

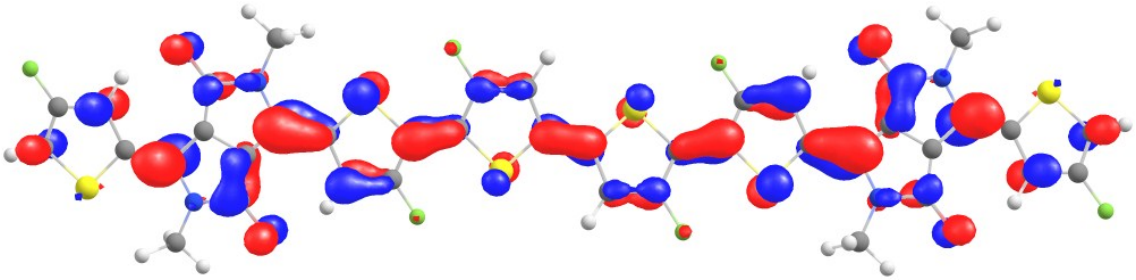

fDT-DPP-4F2Th

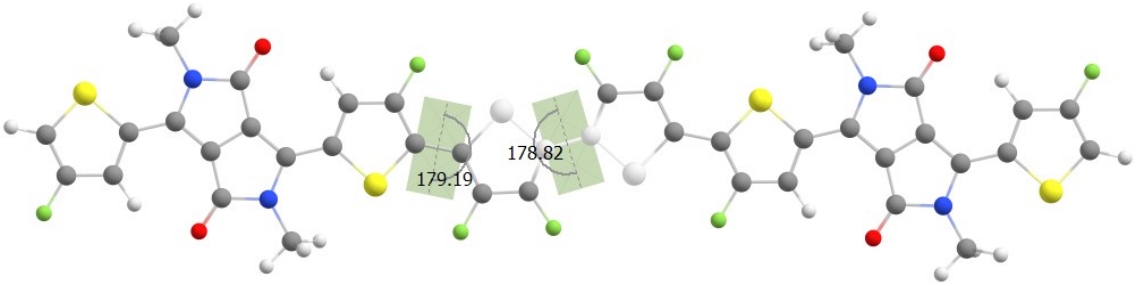

HOMO

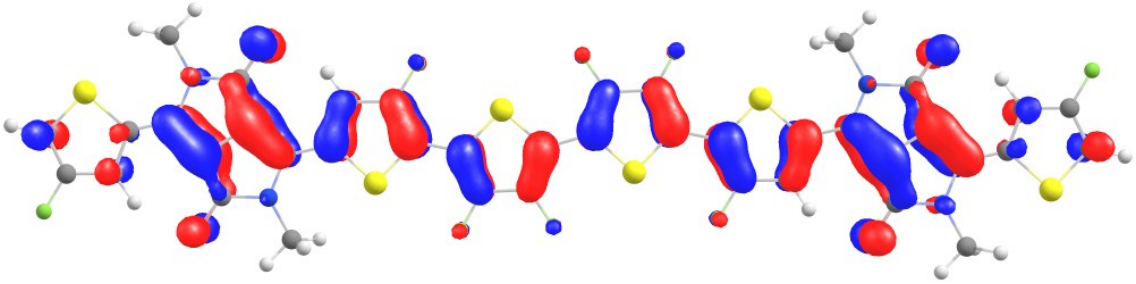

LUMO

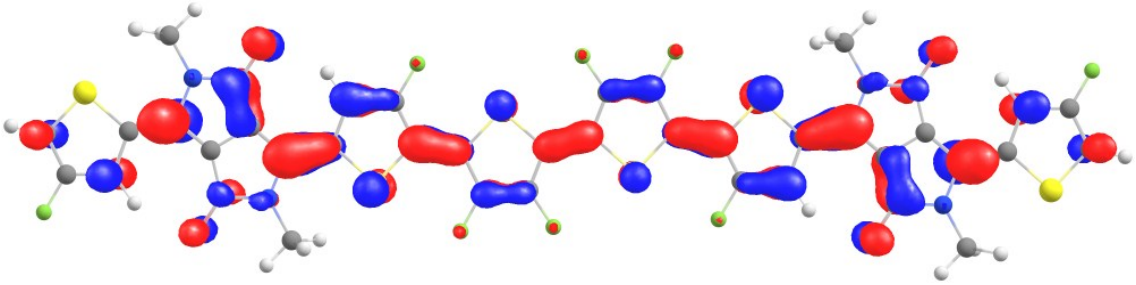

fDT-DPP-2FV2Th

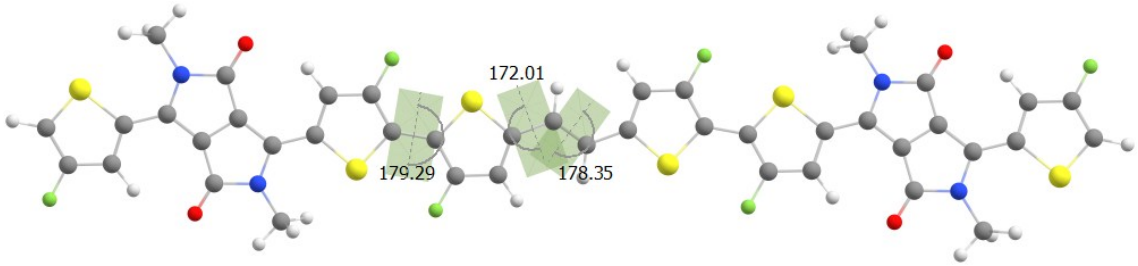

HOMO

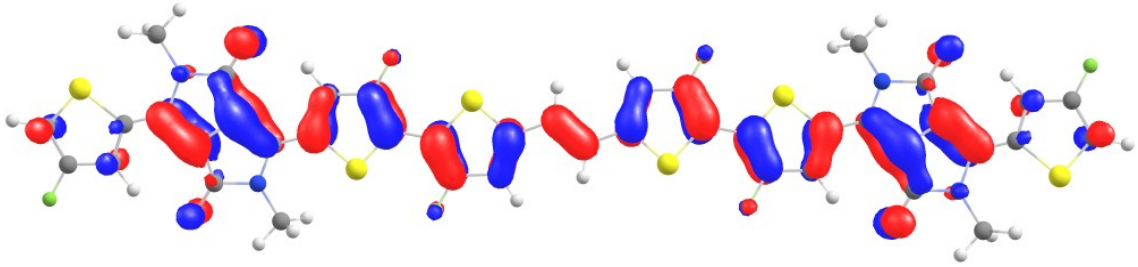

LUMO

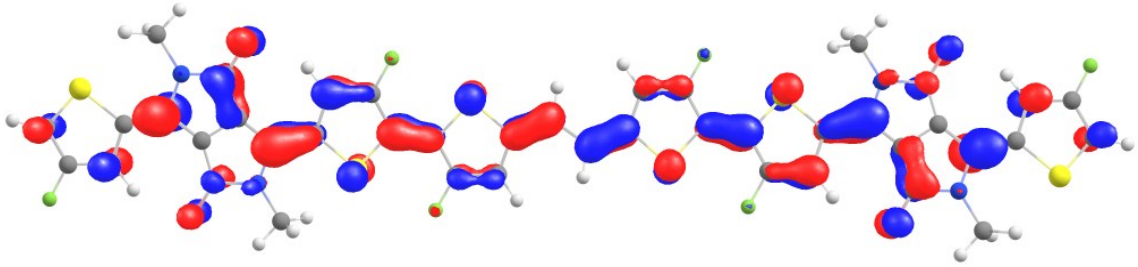

1. Chai, J. D.; Head-Gordon, M. Long-Range Corrected Hybrid Density Functionals with Damped Atom-Atom Dispersion Corrections.Phys. Chem. Chem. Phys.2008,10, 6615−6620.

2. M. J. Frisch, G. W. Trucks, H. B. Schlegel, G. E. Scuseria, M. A. Robb, J. R. Cheeseman, G. Scalmani, V. Barone, G. A. Petersson, H. Nakatsuji, X. Li, M. Caricato, A. V. Marenich, J. Bloino, B. G. Janesko, R. Gomperts, B. Mennucci, H. P. Hratchian, J. V. Ortiz, A. F. Izmaylov, J. L. Sonnenberg, D. Williams-Young, F. Ding, F. Lipparini, F. Egidi, J. Goings, B. Peng, A. Petrone, T. Henderson, D. Ranasinghe, V. G. Zakrzewski, J. Gao, N. Rega, G. Zheng, W. Liang, M. Hada, M. Ehara, K. Toyota, R. Fukuda, J. Hasegawa, M. Ishida, T. Nakajima, Y. Honda, O. Kitao, H. Nakai, T. Vreven, K. Throssell, J. A. Montgomery, Jr., J. E. Peralta, F. Ogliaro, M. J. Bearpark, J. J. Heyd, E. N. Brothers, K. N. Kudin, V. N. Staroverov, T. A. Keith, R. Kobayashi, J. Normand, K. Raghavachari, A. P. Rendell, J. C. Burant, S. S. Iyengar, J. Tomasi, M. Cossi, J. M. Millam, M. Klene, C. Adamo, R. Cammi, J. W. Ochterski, R. L. Martin, K. Morokuma, O. Farkas, J. B. Foresman, and D. J. Fox, Gaussian, Inc., Wallingford CT, 2016.

OFET fabrication

A bottom-contact, bottom-gate OFET configuration was used. Heavily p-doped Si wafer functioned as the gate electrode and a thermally grown SiO_2 layer (~300 nm) with a capacitance of ~10 nF/cm^2 on top of the Si layer was used as the insulating dielectric. Au source, drain and gate electrodes were pre-deposited on the SiO_2 layer with photolithography method and then modified with octadecanthiol. The substrates were cleaned with DI water, acetone, and isopropanol in an ultrasonic bath, followed by O_2 plasma. Subsequently, the substrates were immerged in a dodecyltrichlorosilane (DDTS) solution in toluene (10 mg/mL) at room temperature for 20 min. After washed with toluene, the substrates were dried under a nitrogen flow. A polymer solution in chloroform (concentration: **P1** and **P2**: 5 mg/mL; **P3**: 2-3 mg/mL) was spin coated on the substrate at 3000 rpm for 60 s to give a film, which was subjected to thermal annealing at different temperature for 20 min in glove box. The channel length (L) and width (W) was 30 and 1000 μm, respectively. The devices were characterized in air using an Agilent B2912A Semiconductor Analyzer. The carrier mobility in the saturated regime, μ_{sat}, was calculated according to the equation of $I_{DS} = C_i\mu_{sat}(W/2L)(V_G-V_T)^2$, where I_{DS} is the drain current, C_i is the capacitance of the gate dielectric, and V_G and V_T are the gate voltage and threshold voltage, respectively. V_T of the devices was determined from extrapolation of the linear fit of the $(I_{DS})^{1/2}$ versus V_G curve in the saturation regime at $I_{DS} = 0$.

Output and transfer curves of OFETs

P1

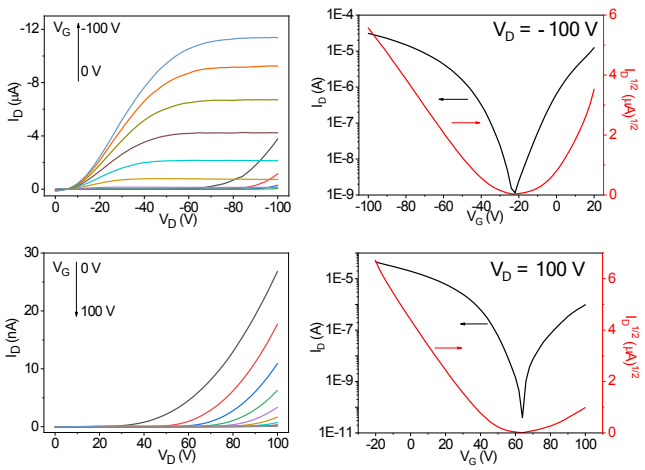

P2

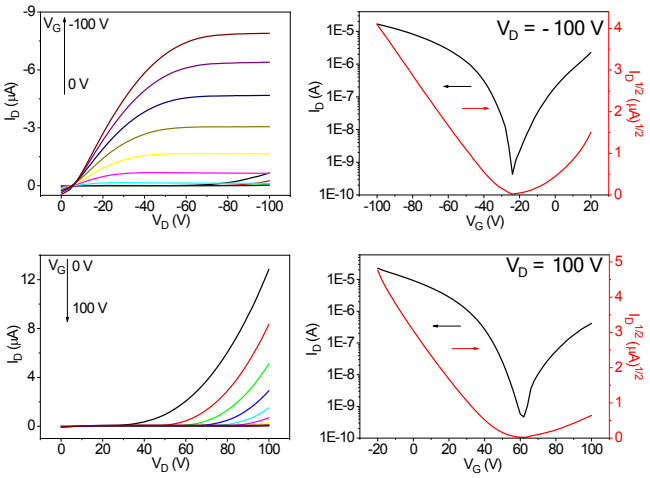

P3

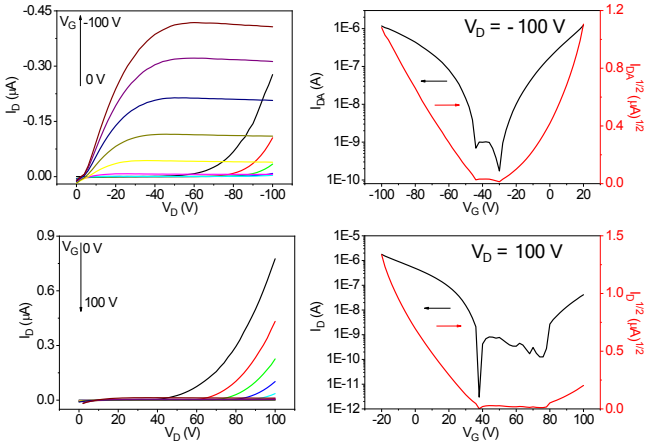

X-ray diffraction

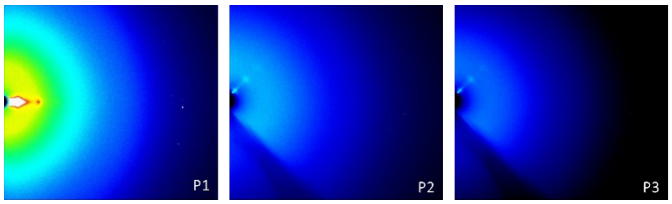

two-dimensional grazing-incidence X-ray diffraction (2D-GIXD) for **P1**, **P2** and **P3**

NMR spectrum

3-bromo-2-(dimethyloctylsyilyl)thiophene (5)

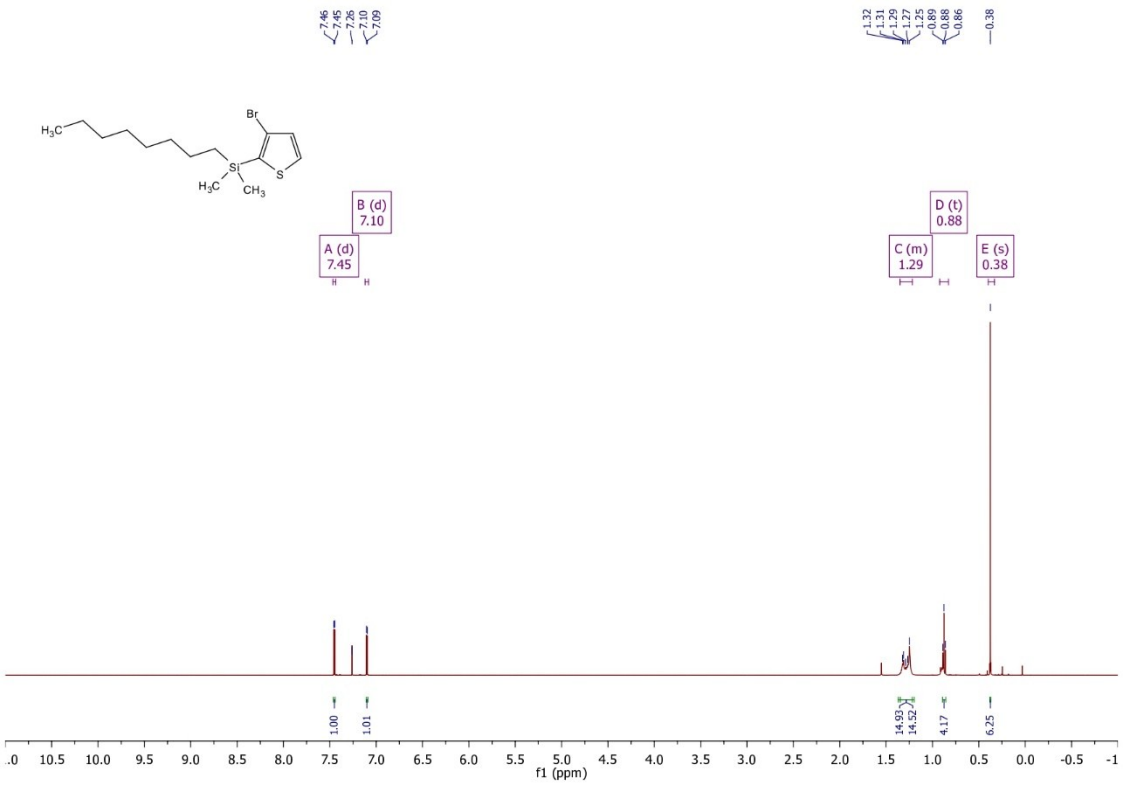

3-fluoro-2-(dimethyloctylsyilyl)thiophene (6)

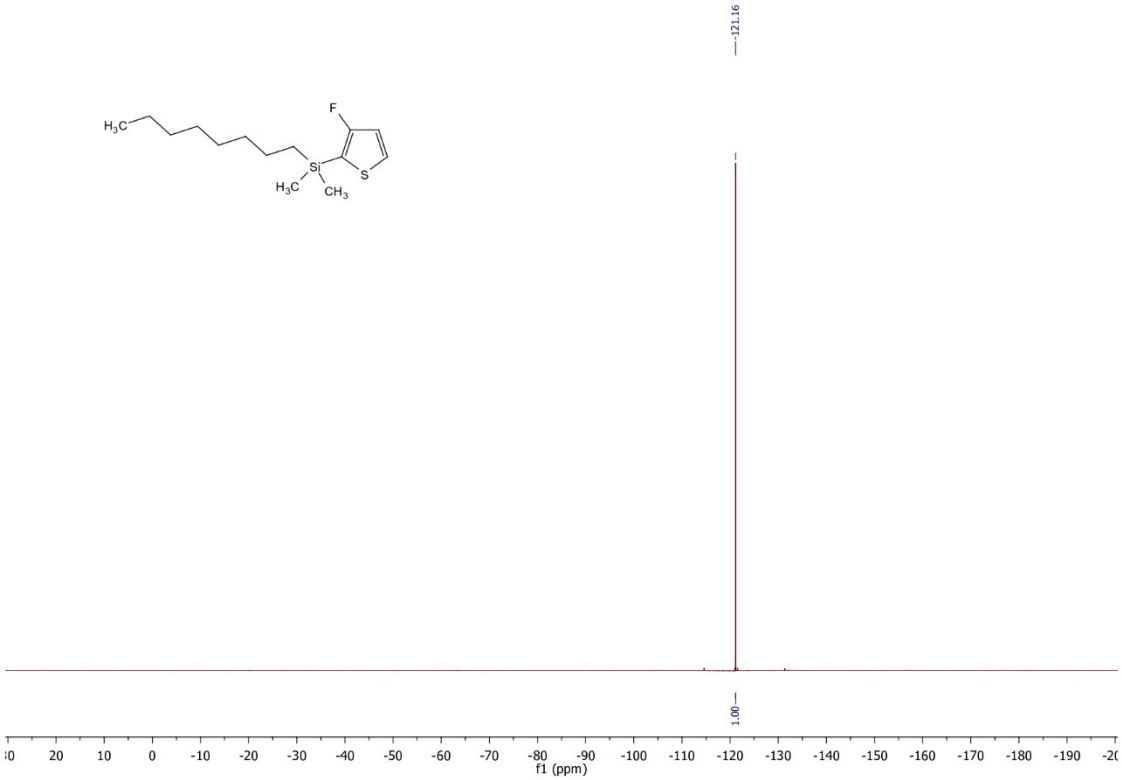

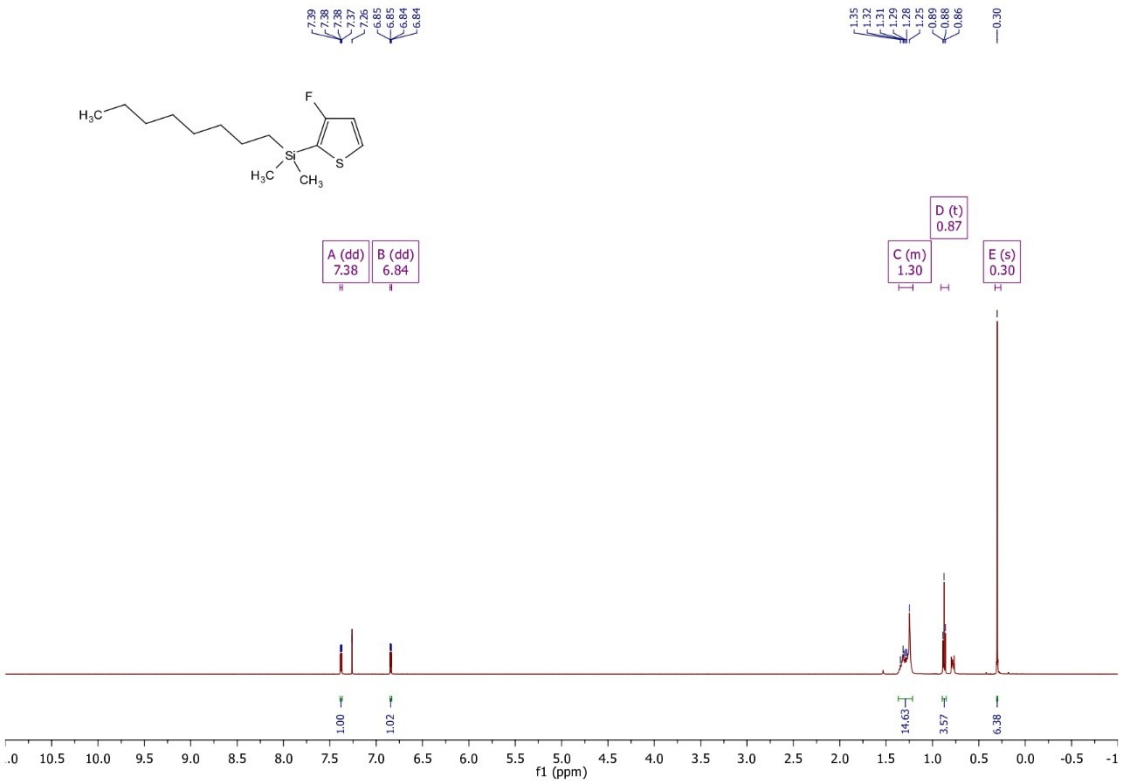

4-fluoro-5-(dimethyloctylsyilyl)-2-thiophenecarbonitrile (7)

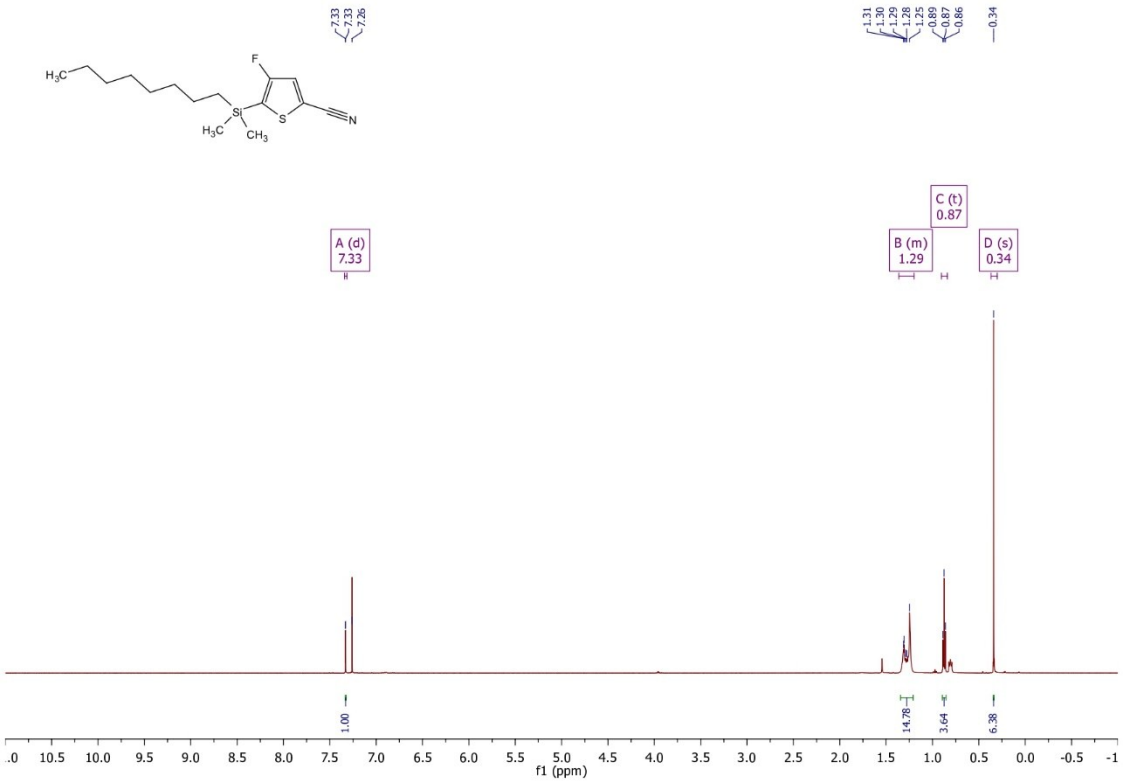

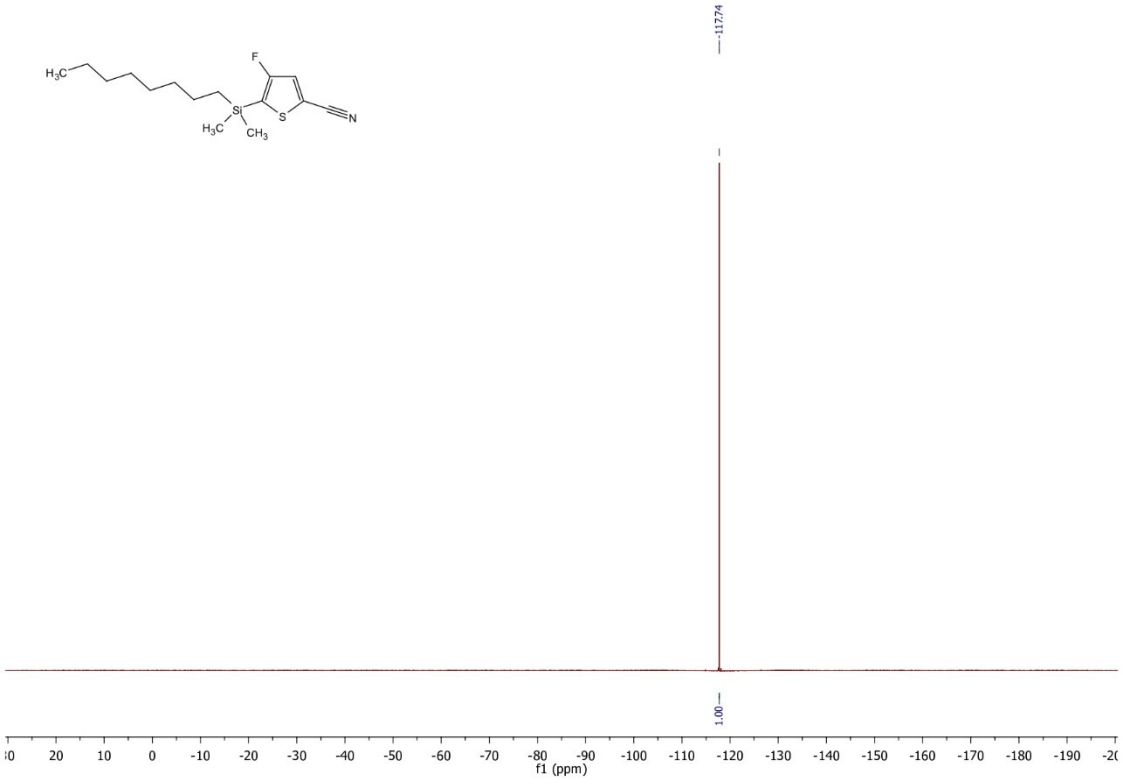

3,6-bis(4-fluorothiophen-2-yl)-2,5-dihydropyrrolo[3,4-c]pyrrole-1,4-dione (fDT-DPP)

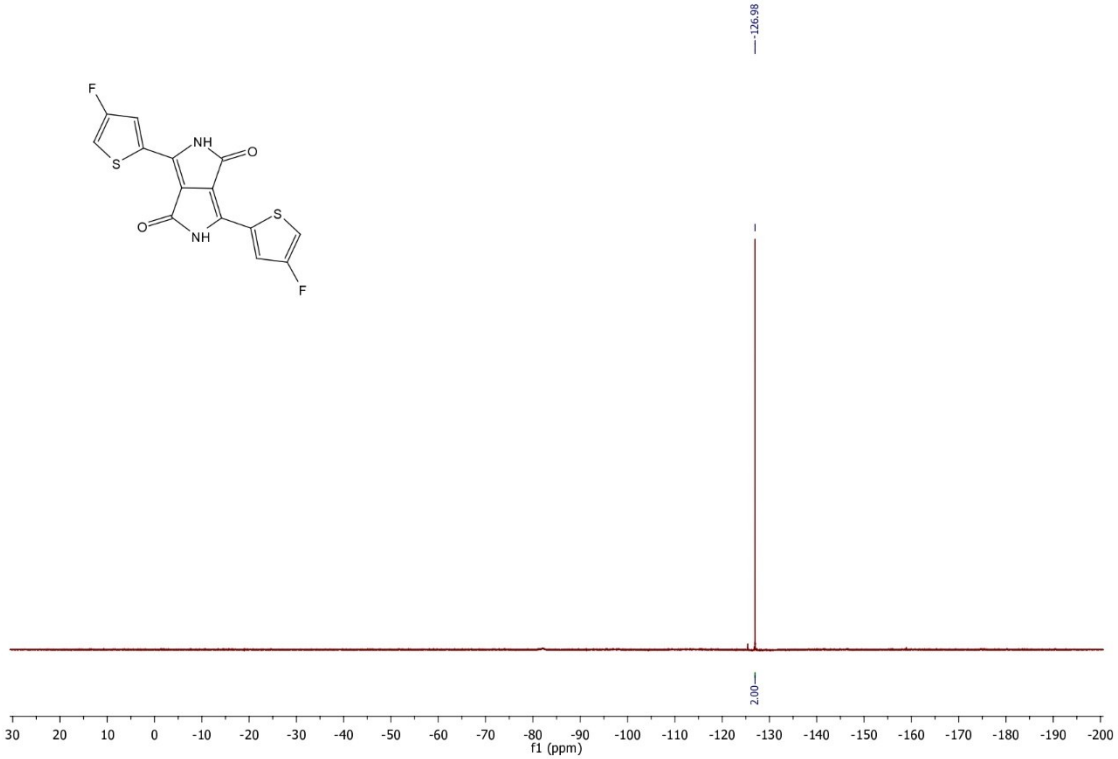

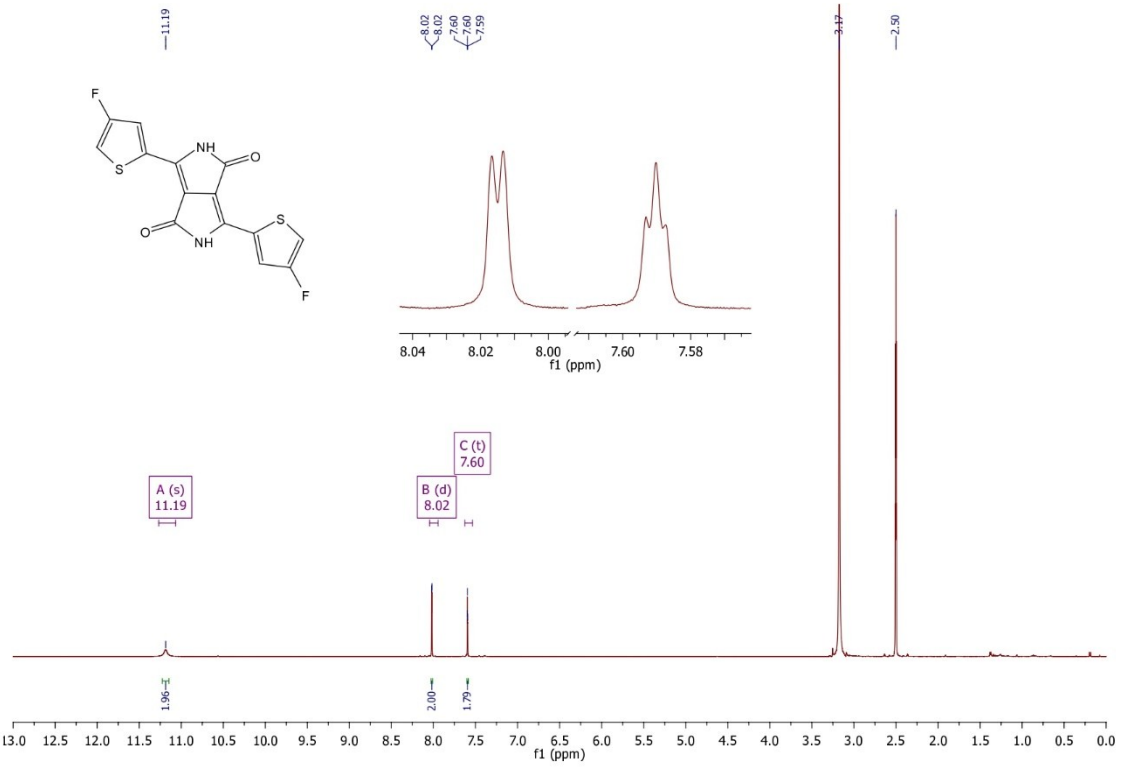

3,6-bis(4-fluorothiophen-2-yl)-2,5-bis(4-octadecyldocosyl)-2,5-dihydropyrrolo[3,4-c]pyrrole-1,4-dione (8a)

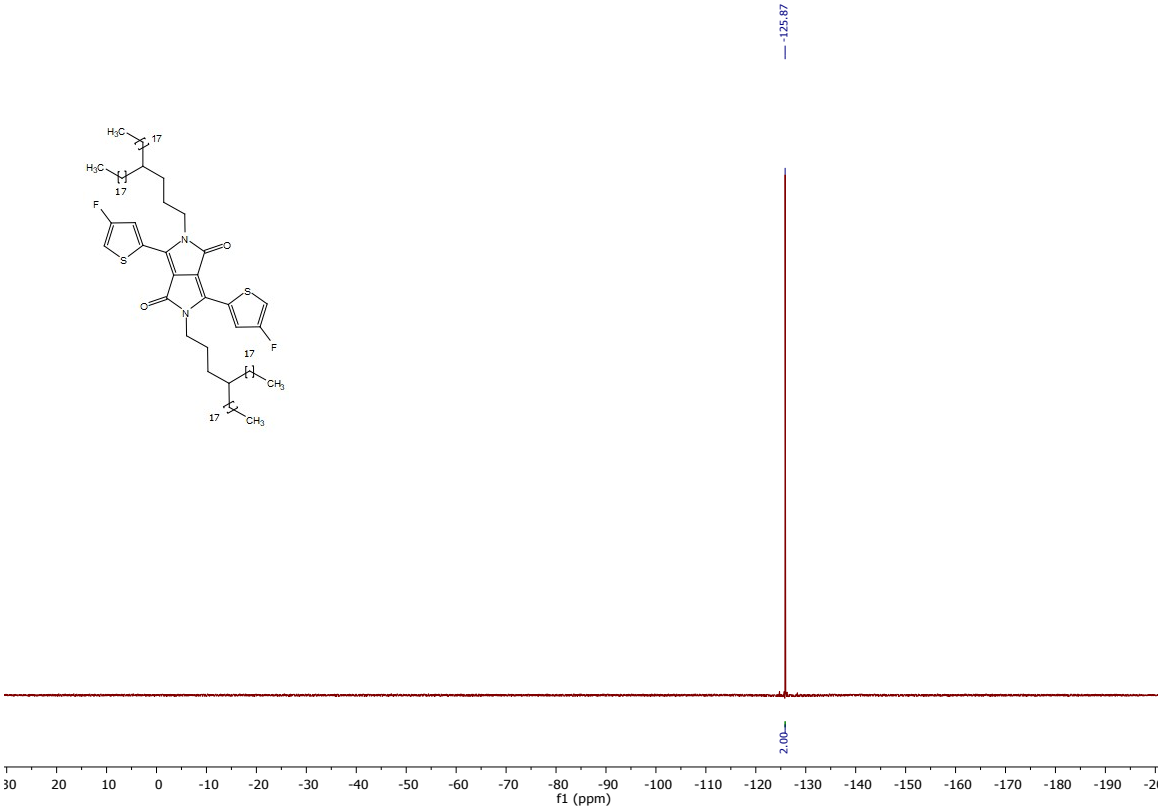

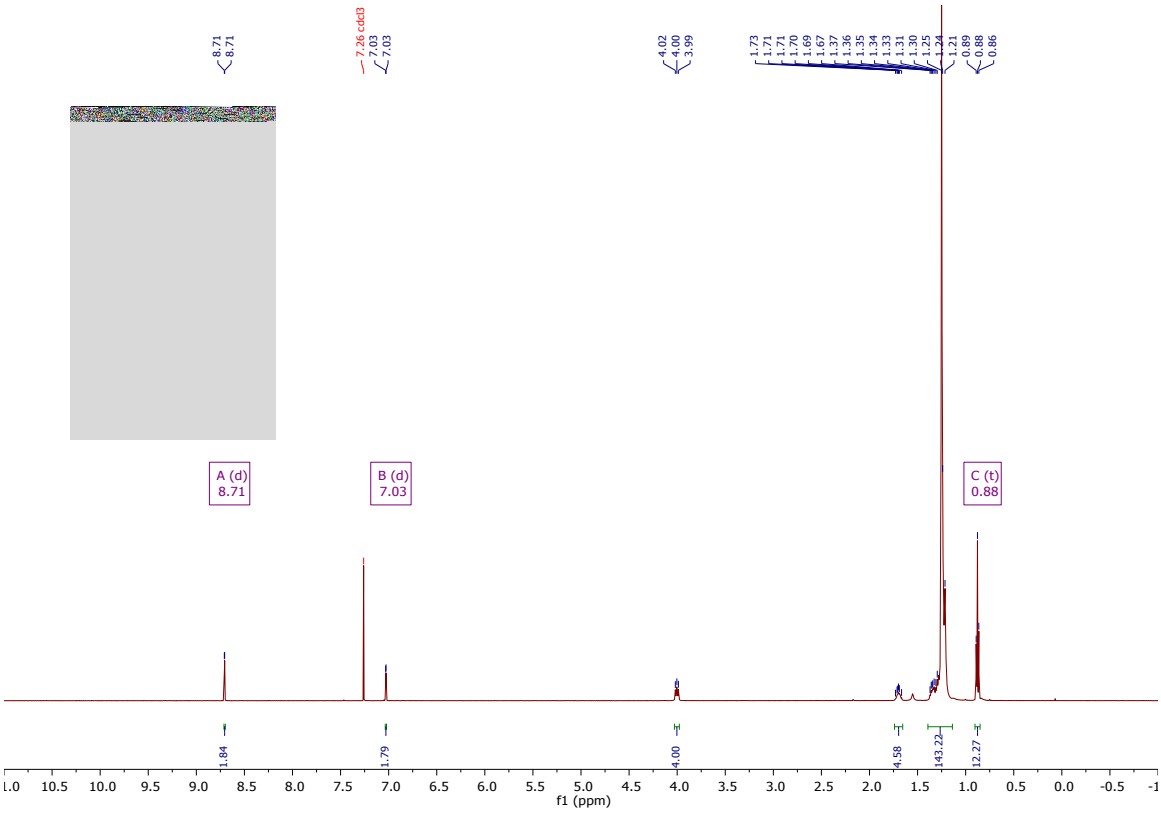
8.71
8.71
7.26 cdcl3
7.03
7.03
4.02
4.00
3.99
1.73
1.71
1.71
1.70
1.69
1.67
1.37
1.36
1.35
1.34
1.33
1.31
1.30
1.25
1.24
1.21
0.89
0.88
0.86
A (d)
8.71
B (d)
7.03
C (t)
0.88
1.84
1.79
4.00
4.58
143.22
12.27
f1 (ppm)

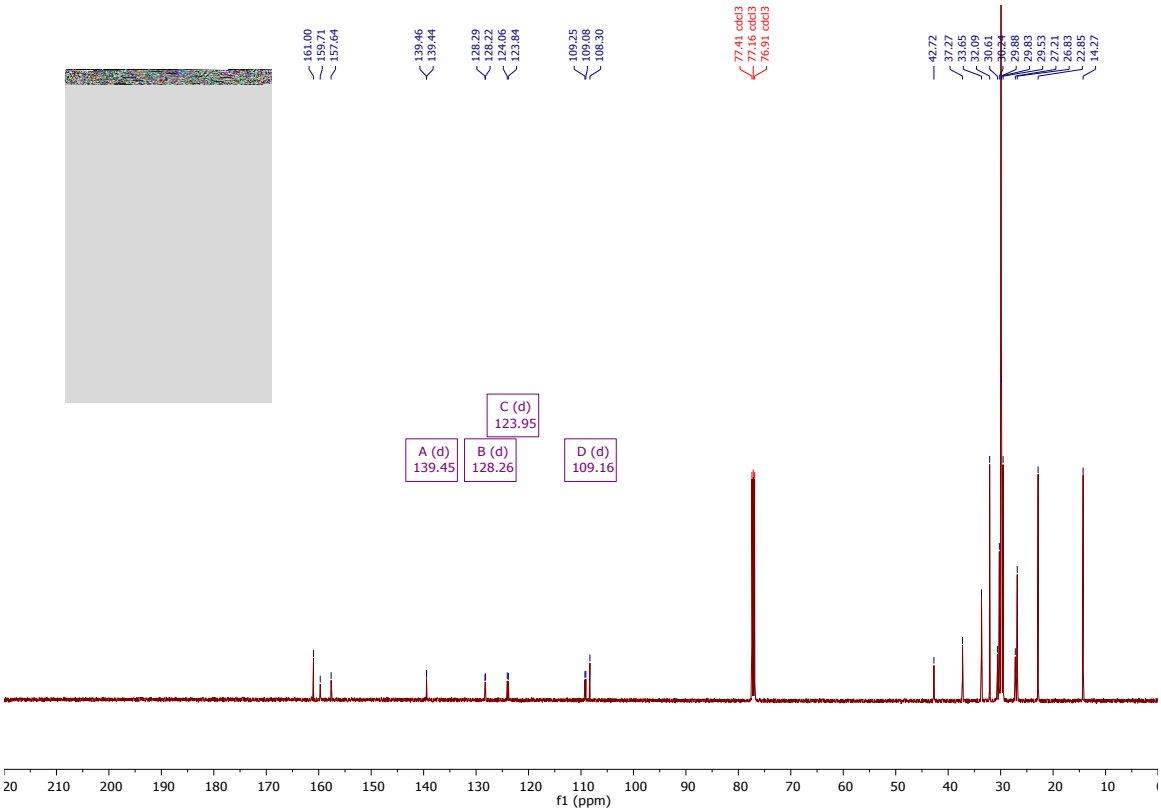
161.00
159.71
157.64
139.46
139.44
128.29
128.22
124.06
123.84
109.25
109.08
108.30
77.41 cdcl3
77.16 cdcl3
76.91 cdcl3
42.72
37.27
33.65
32.09
30.61
30.24
29.88
29.83
29.53
27.21
26.83
22.85
14.27
C (d)
123.95
A (d)
139.45
B (d)
128.26
D (d)
109.16
f1 (ppm)

3,6-bis(4-fluorothiophen-2-yl)-2,5-bis(4-tetradecyloctadecyl)-2,5-dihydropyrrolo[3,4-c]pyrrole-1,4-dione (8b)

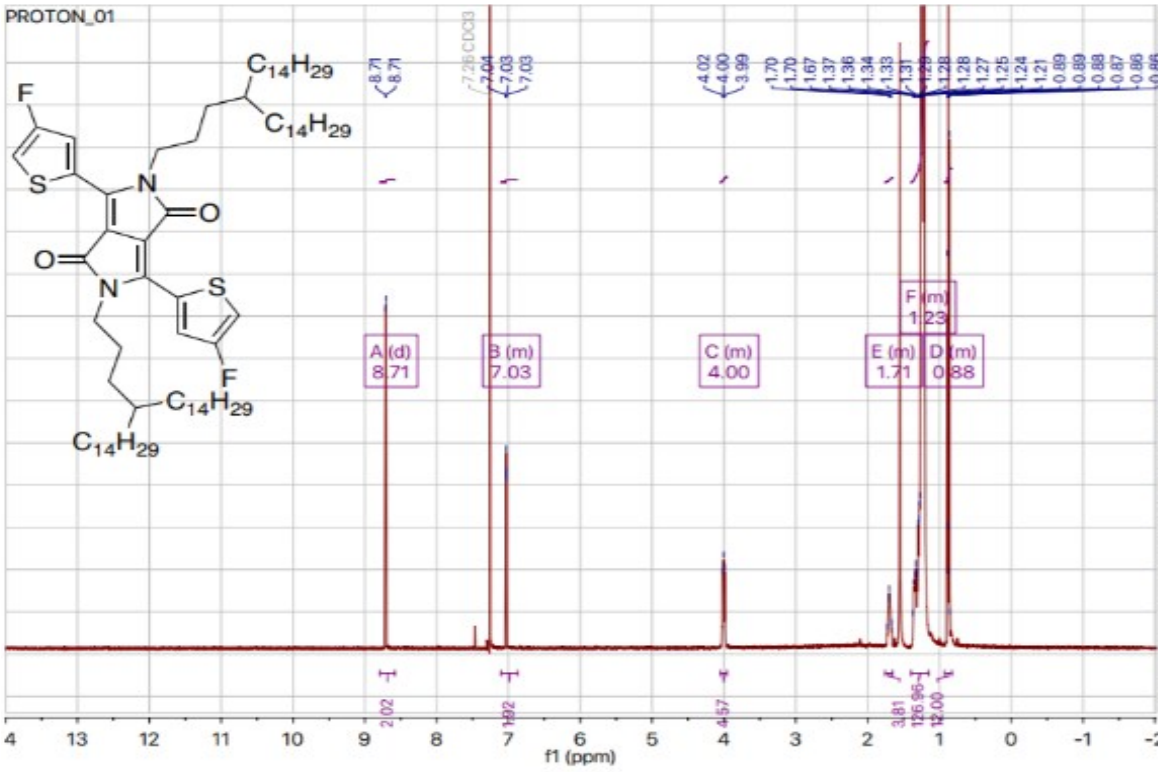

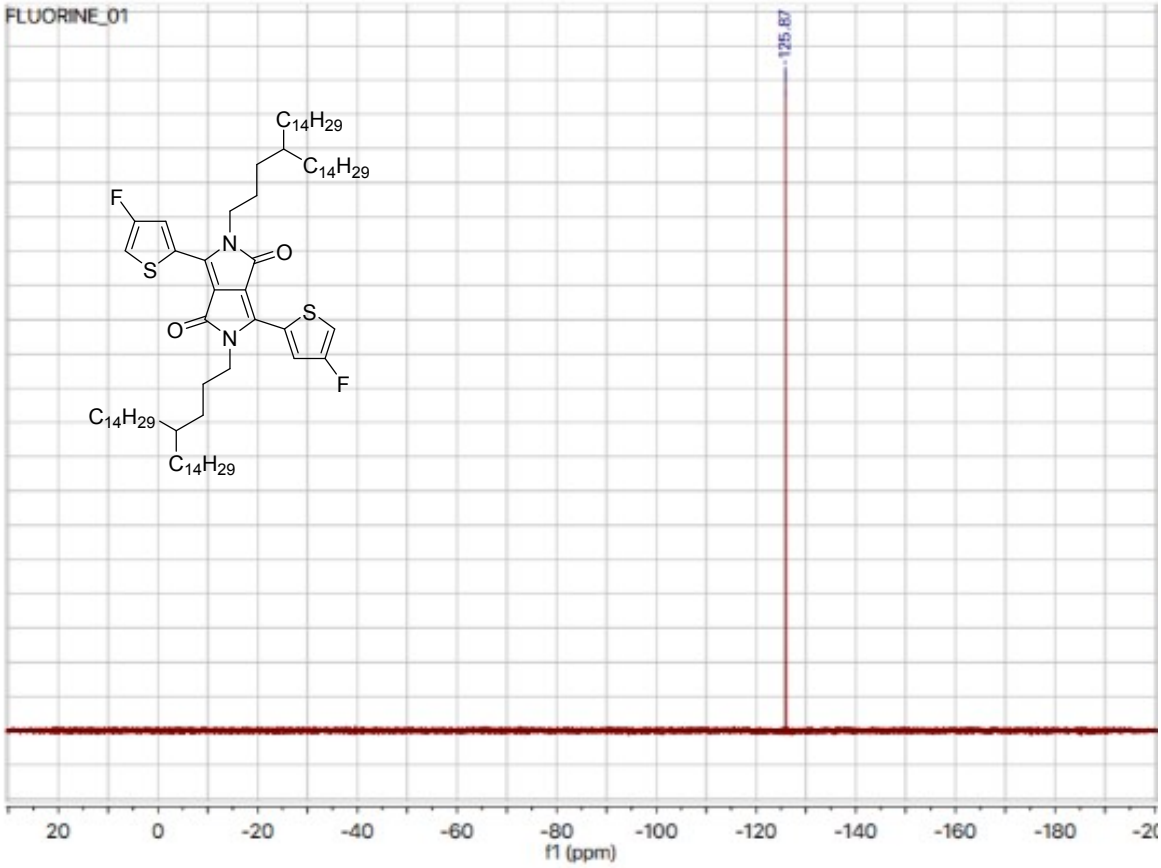
FLUORINE_01
125.87
C14H29
C14H29
F
S
N
O
O
N
S
F
C14H29
C14H29
20
0
-20
-40
-60
-80
-100
-120
-140
-160
-180
f1 (ppm)

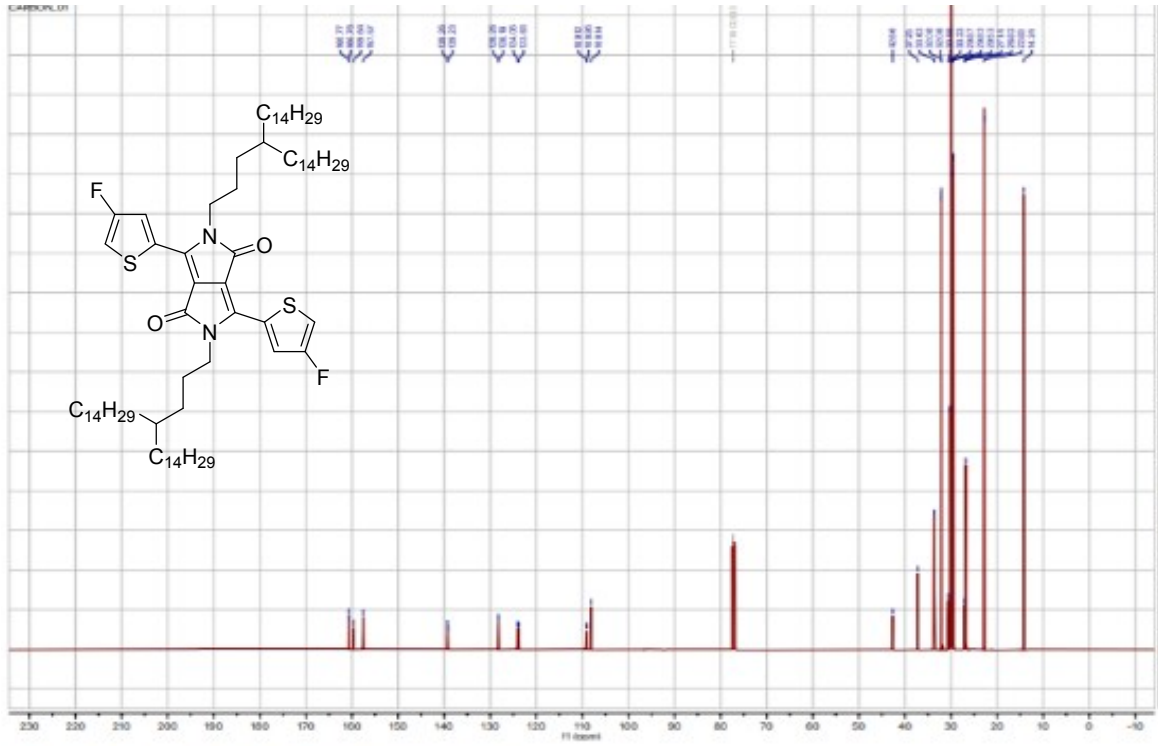
C14H29
C14H29
F
S
N
O
O
N
S
F
C14H29
C14H29

3,6-bis(5-bromo-4-fluorothiophen-2-yl)-2,5-bis(4-octadecyldocosyl)-2,5-dihydropyrrolo[3,4-c]pyrrole-1,4-dione (9a)

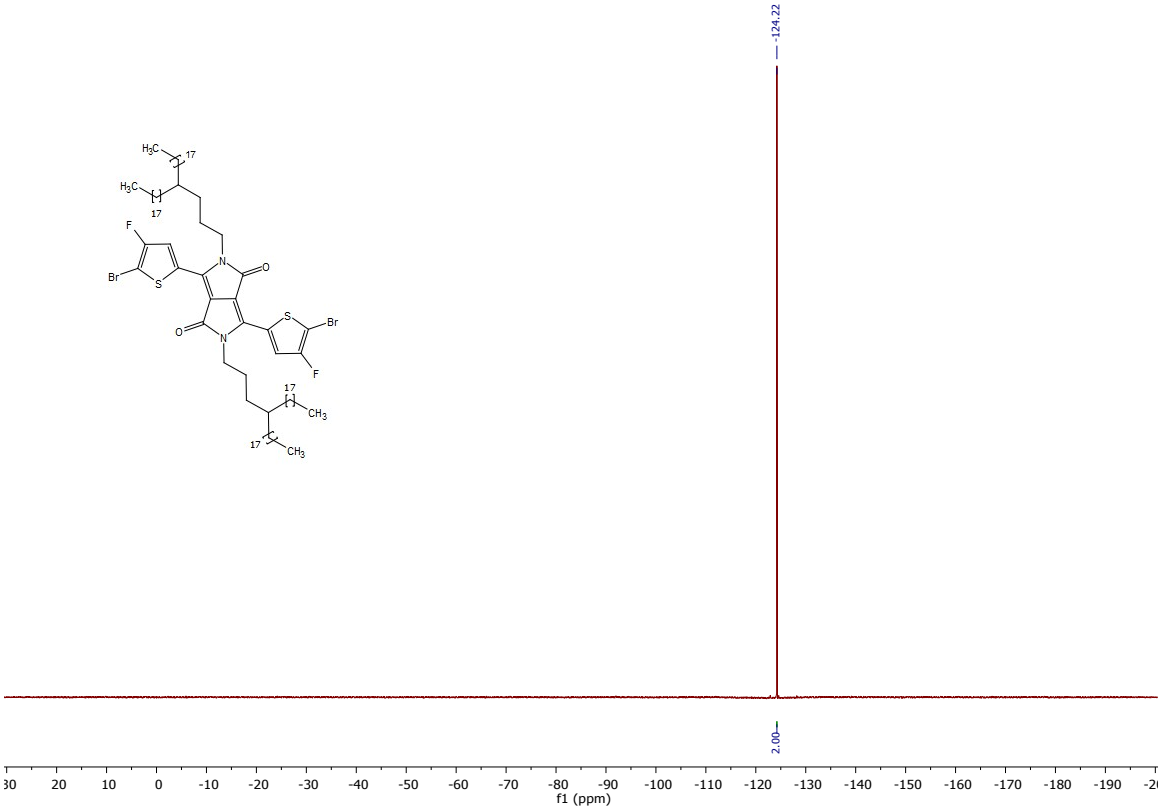

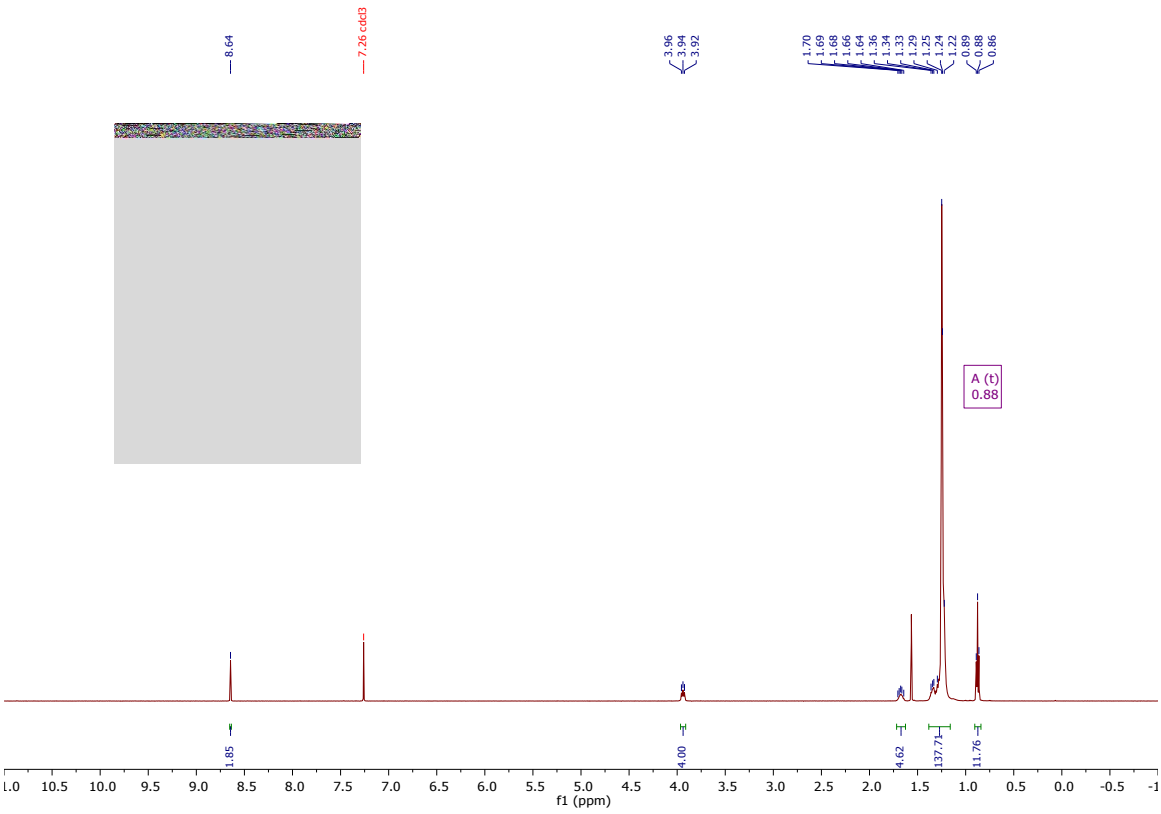
8.64
7.26 cdcl3
3.96
3.94
3.92
1.70
1.69
1.68
1.66
1.64
1.36
1.34
1.33
1.29
1.25
1.24
1.22
0.89
0.88
0.86
A (t)
0.88
1.85
4.00
4.62
137.71
11.76
f1 (ppm)

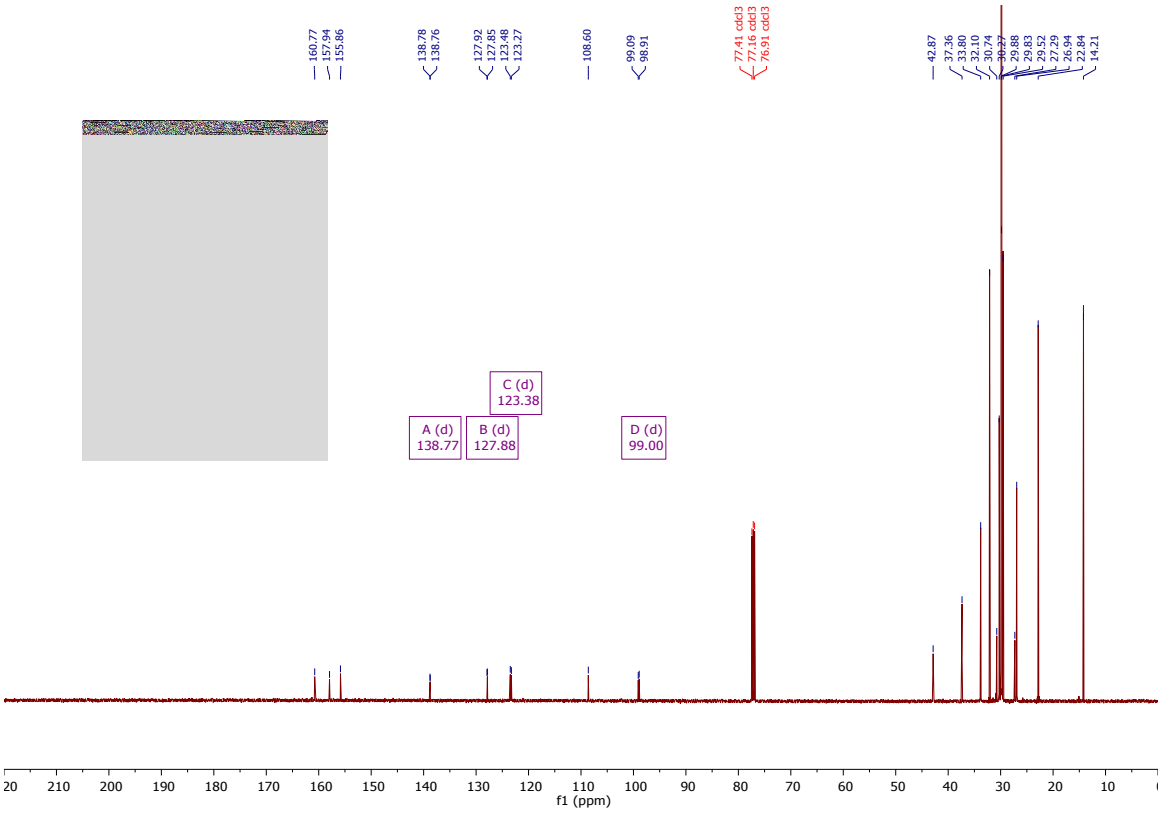

3,6-bis(5-bromo-4-fluorothiophen-2-yl)-2,5-bis(4-tetradecyloctadecyl)-2,5-dihydropyrrolo[3,4-c]pyrrole-1,4-dione
(9b)

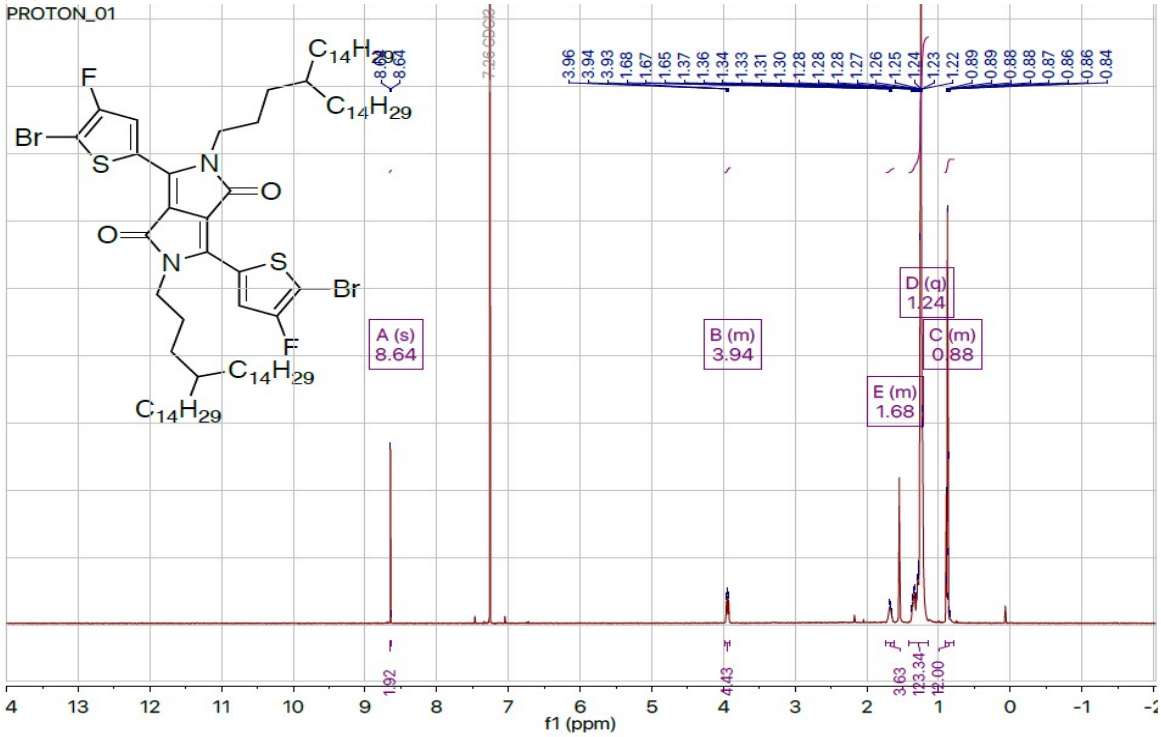

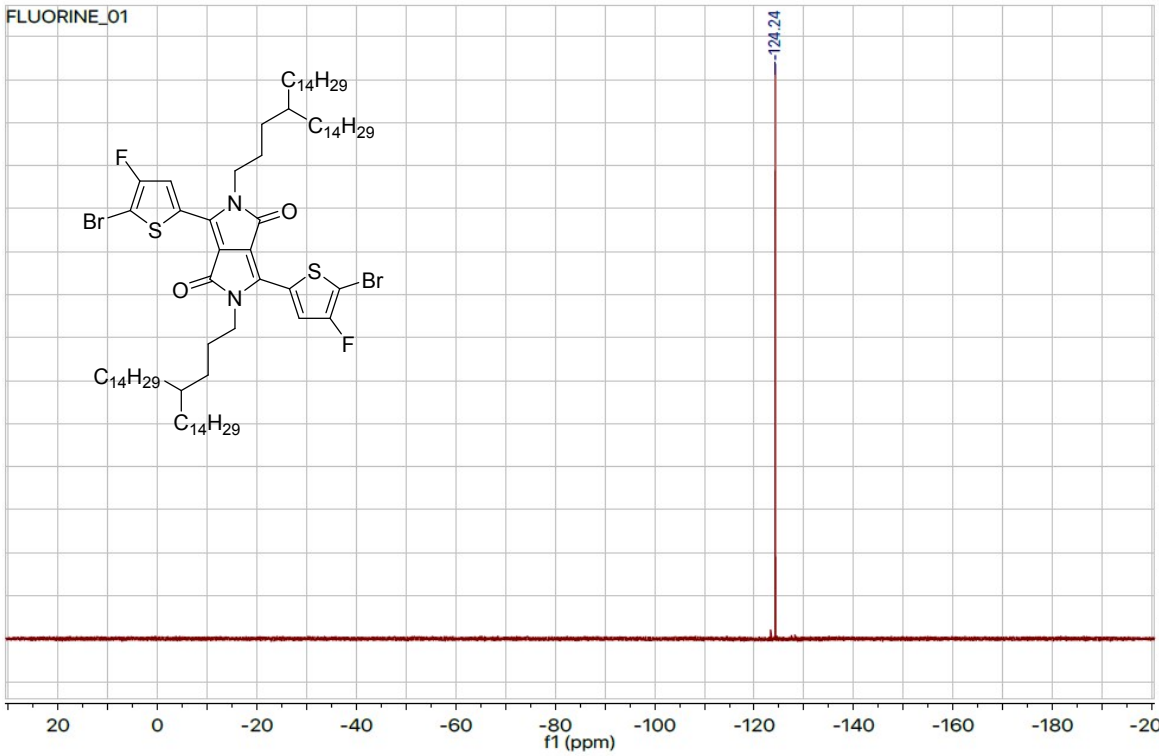
FLUORINE_01
-124.24
20
0
-20
-40
-60
-80
-100
-120
-140
-160
-180
f1 (ppm)

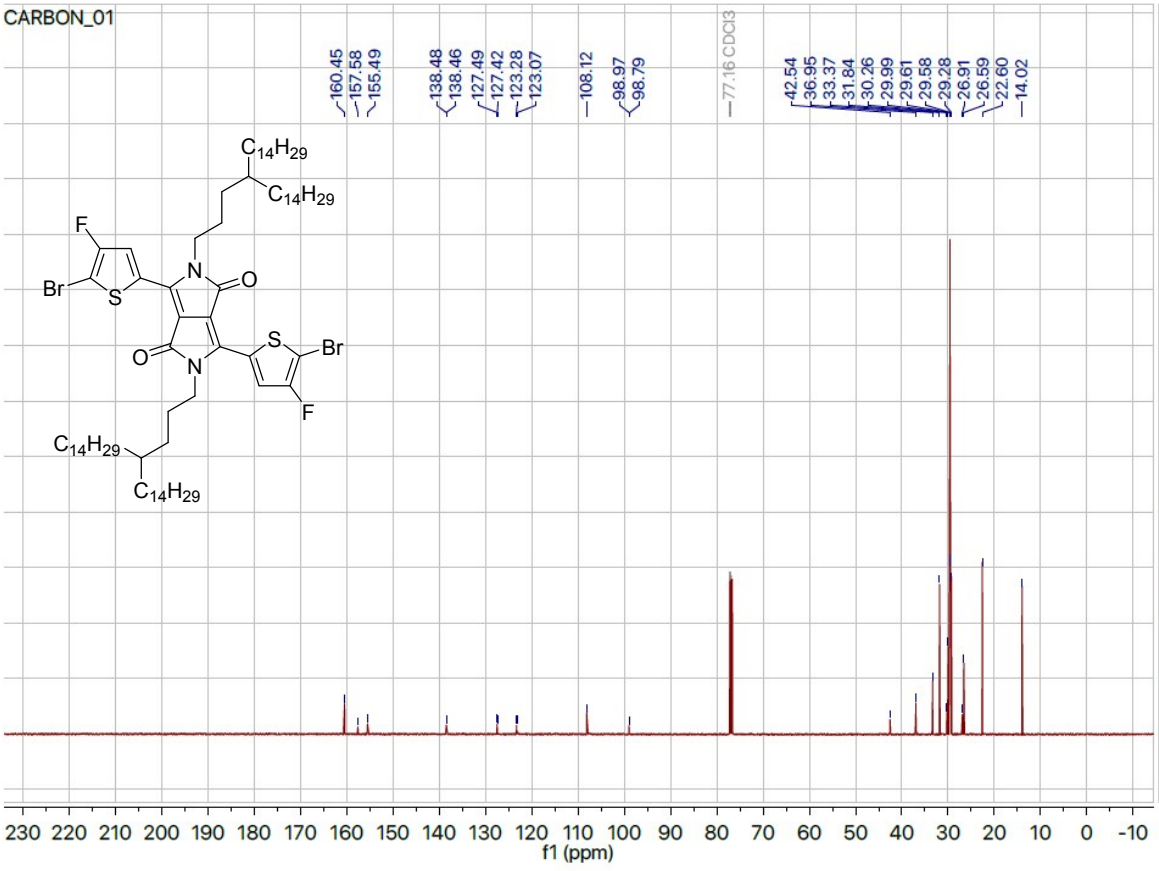
CARBON_01
160.45
157.58
155.49
138.48
138.46
127.49
127.42
123.28
123.07
108.12
98.97
98.79
77.16 CDCl3
42.54
36.95
33.37
31.84
30.26
29.99
29.61
29.58
29.28
26.91
26.59
22.60
14.02
230 220 210 200 190 180 170 160 150 140 130 120 110 100 90 80 70 60 50 40 30 20 10 0 -10
f1 (ppm)

4,4'-difluoro-2,2'-bithiophene (10)

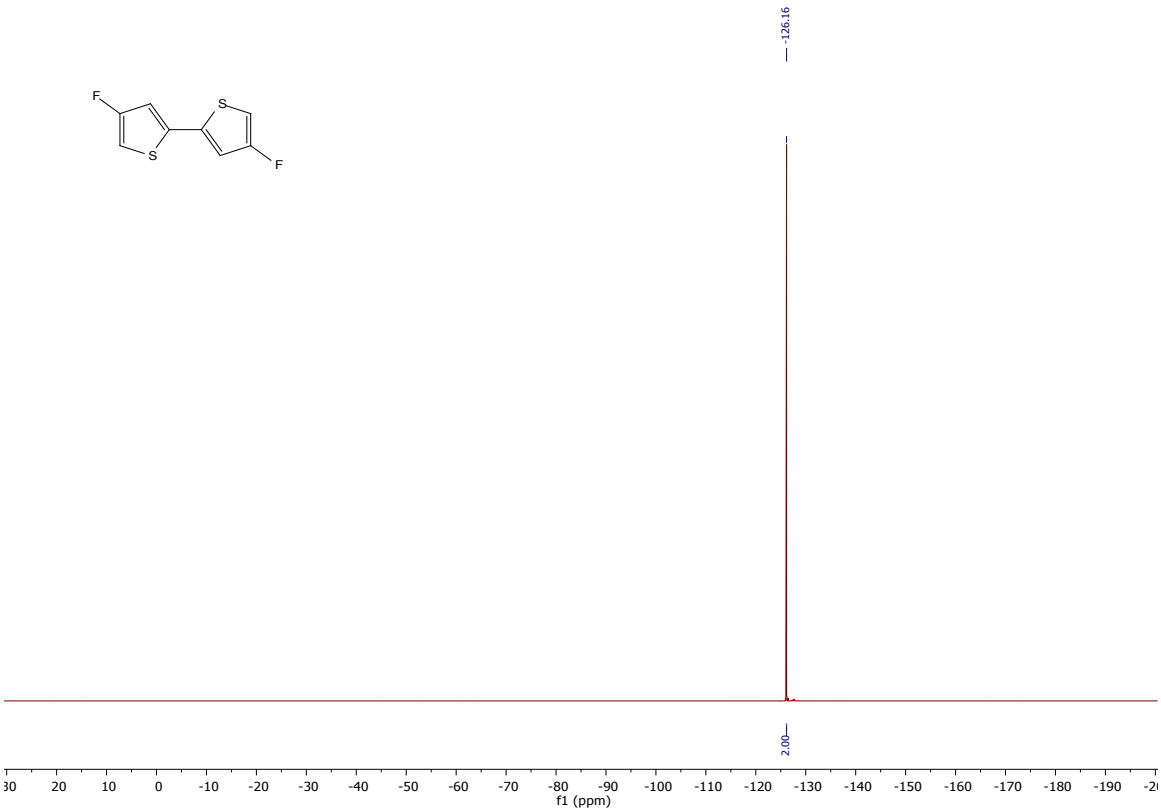

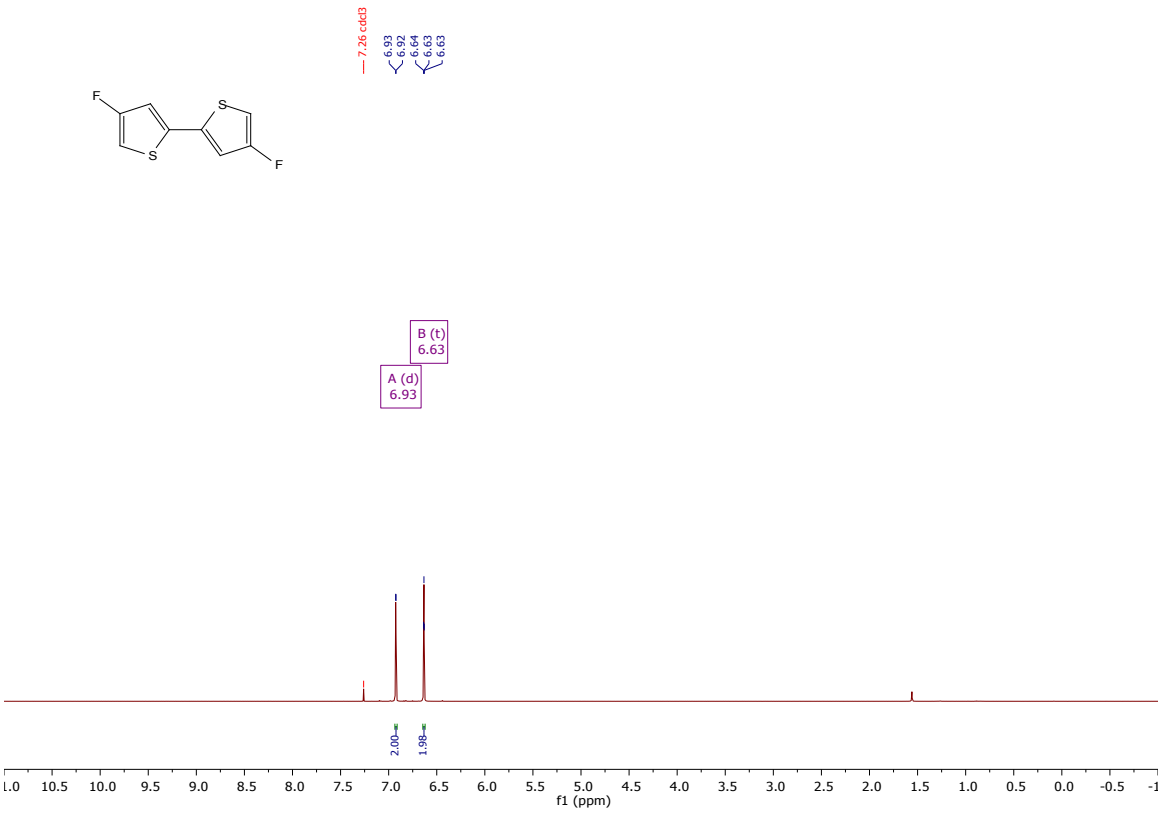
7.26 cdd3
6.93
6.92
6.64
6.63
6.63
F
S
S
F
B (t)
6.63
A (d)
6.93
2.00
1.98
f1 (ppm)

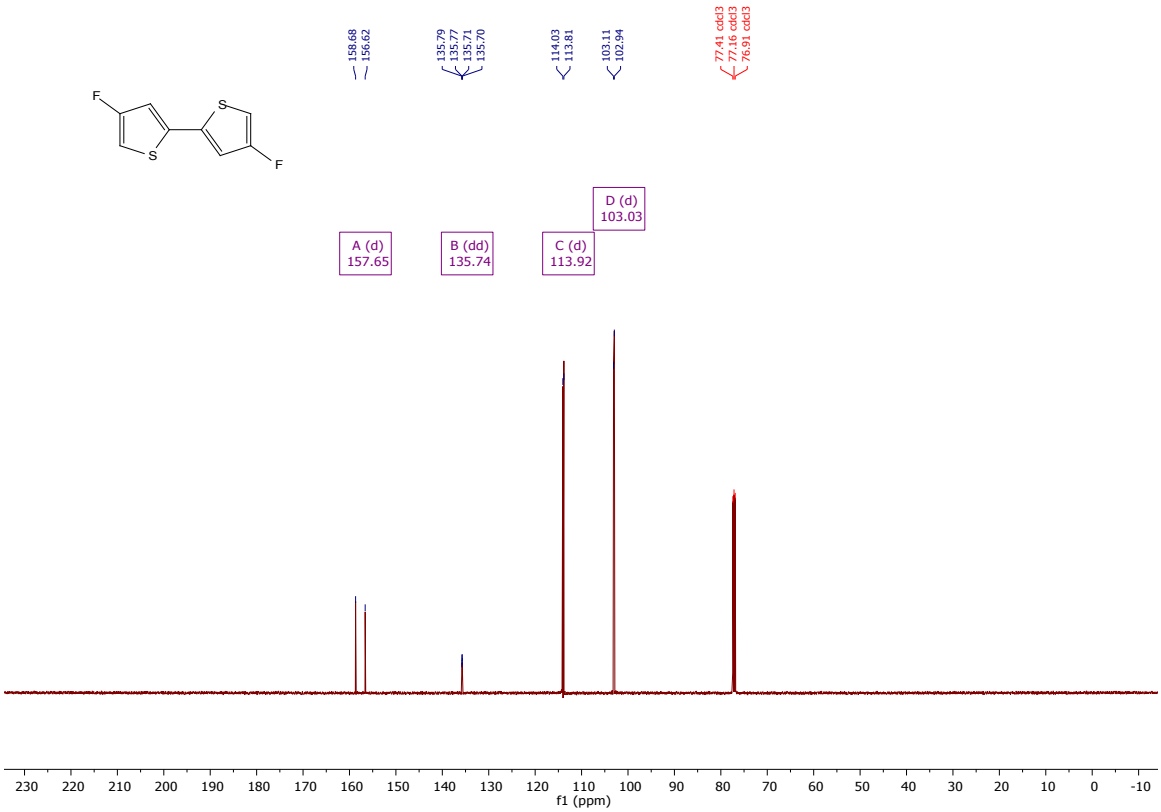

5-(dimethyl(octyl)silyl)-4-fluorothiophene-2-carbaldehyde (11)

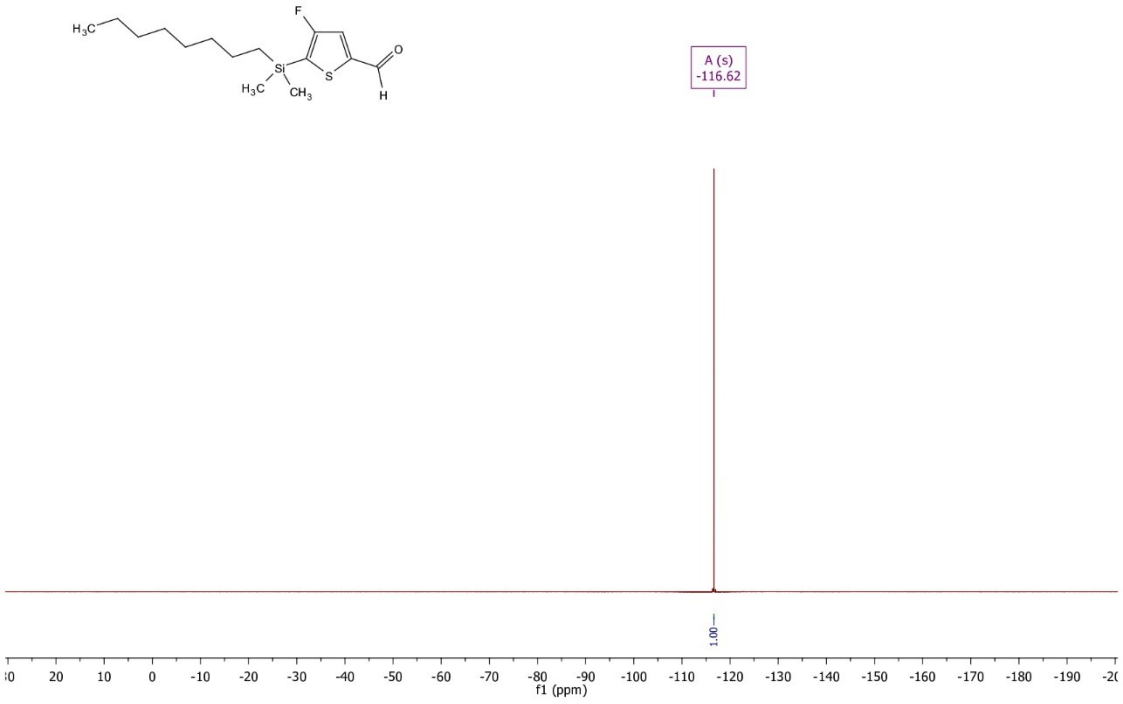

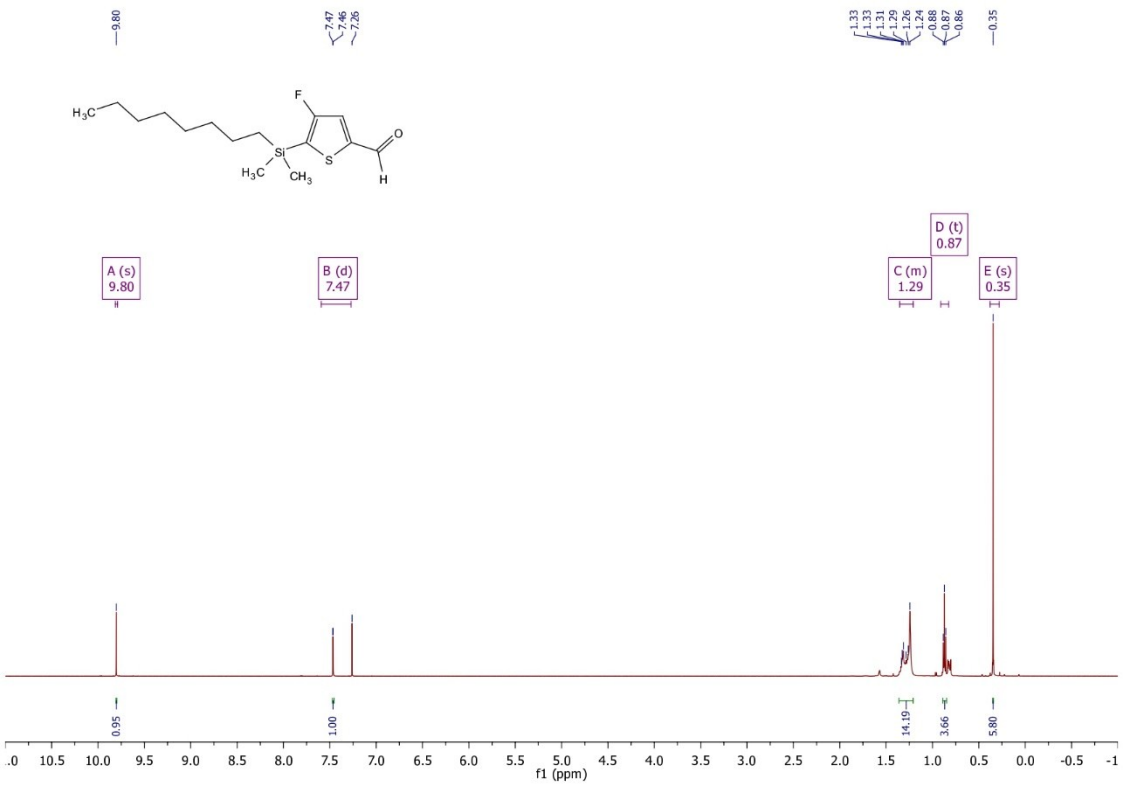

(E)-1,2-bis(4-fluorothiophen-2-yl)ethene (12)

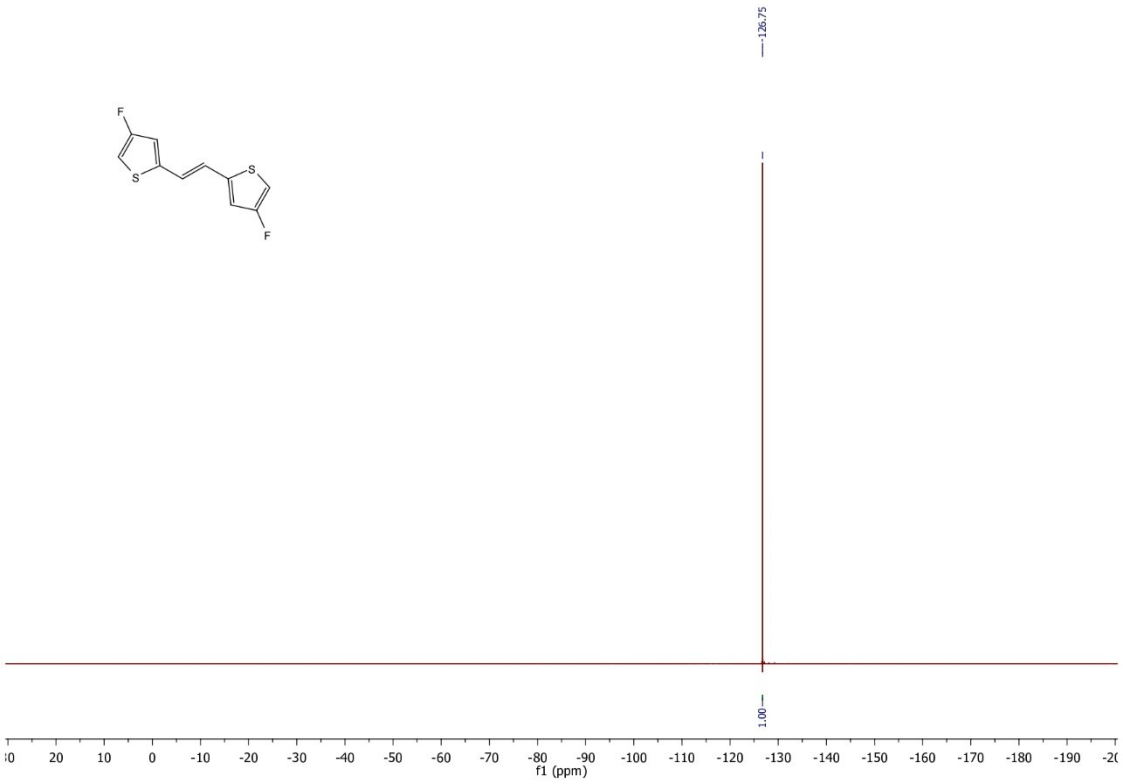

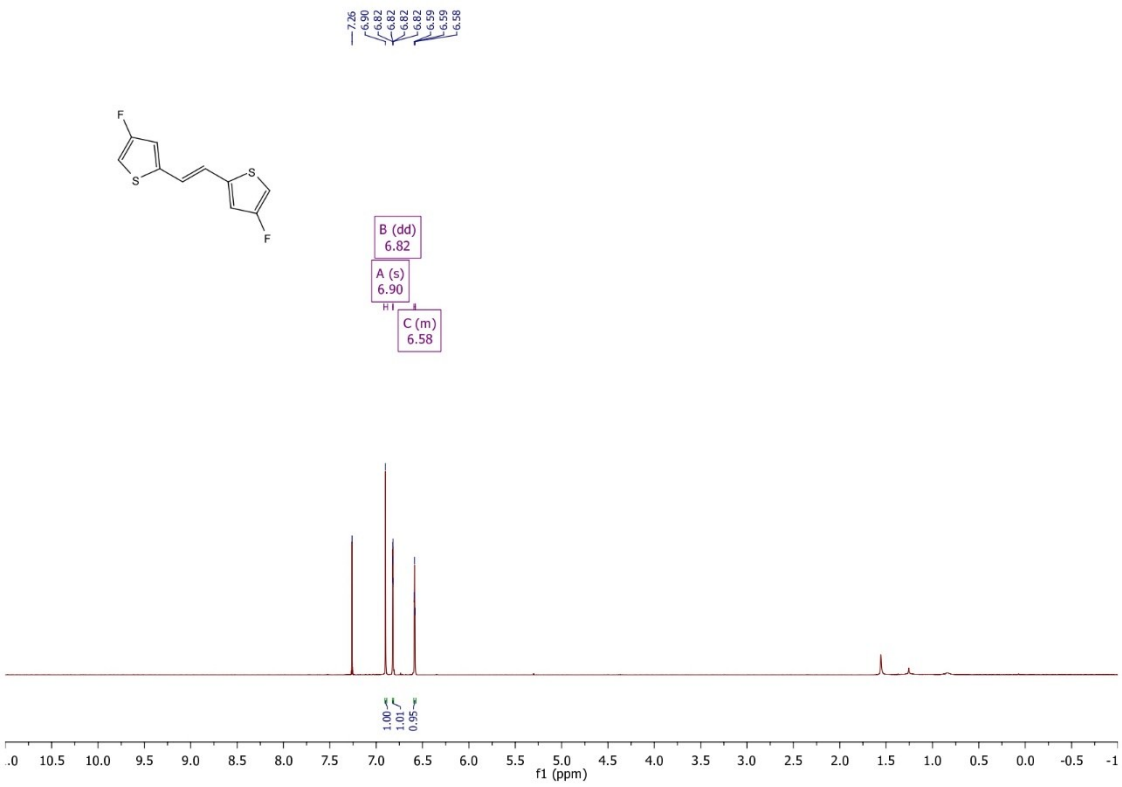

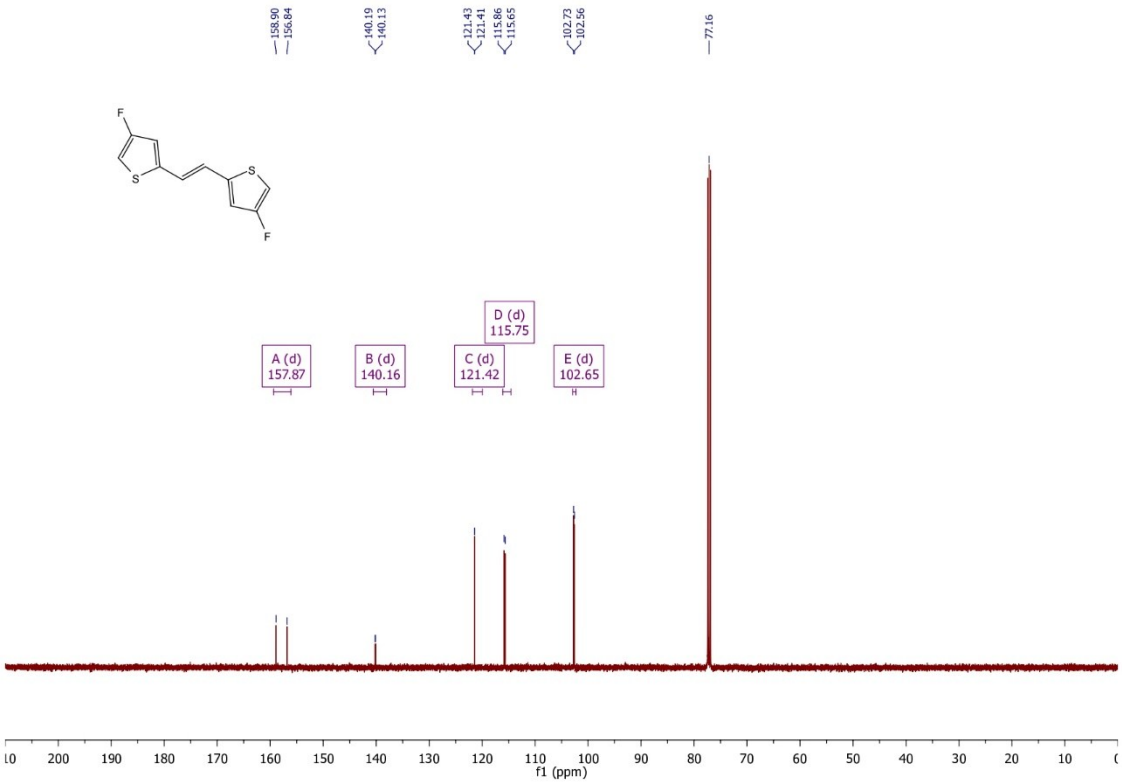

3,3',4,4'-tetrafluoro-2,2'-bithiophene (14)

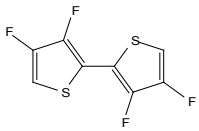
F
F
S
S
F
F

-134.96
-134.99
-136.38
-136.40
B (d)
-136.39
A (d)
-134.98
2.00
1.98
f1 (ppm)

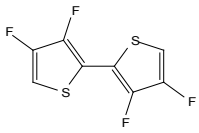
F
F
S
S
F
F

7.26 cdcl3
6.78
6.77
6.77
6.77
6.76
6.76
6.76
6.76
6.75
6.75
A (m)
6.76
2.00
f1 (ppm)

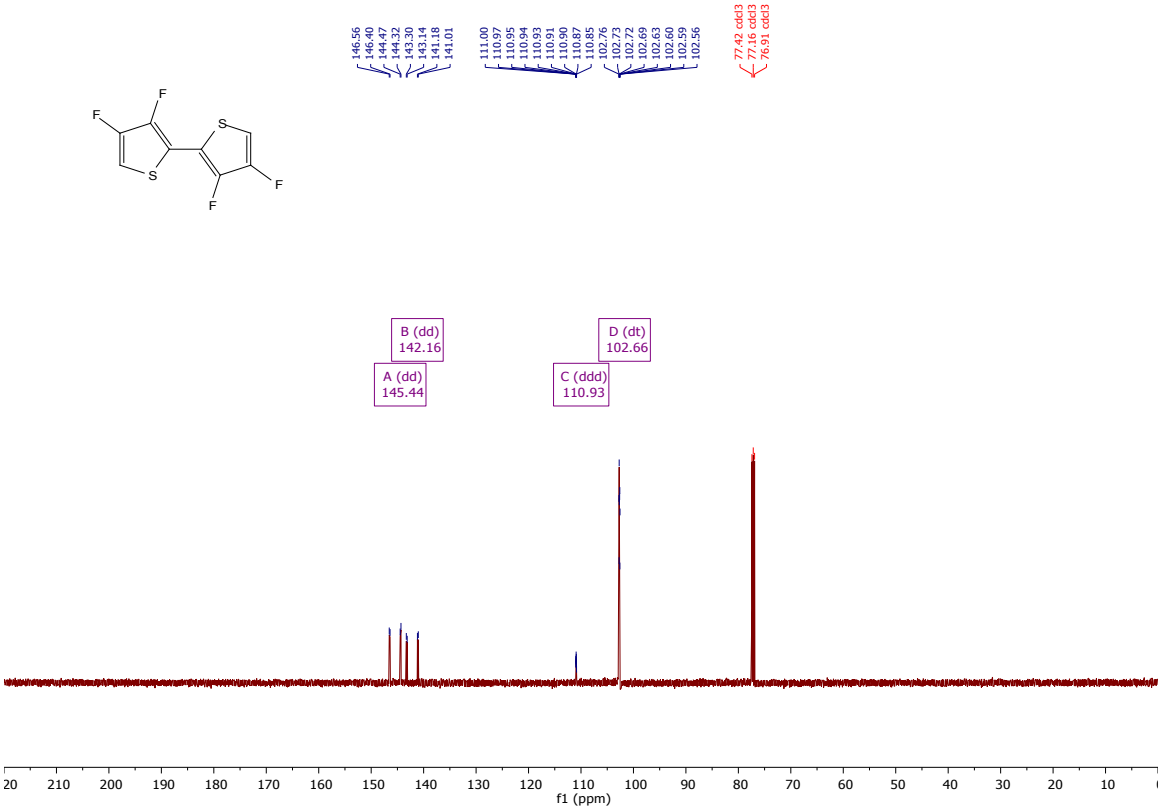
146.56
146.40
144.47
144.32
143.30
143.14
141.18
141.01
111.00
110.97
110.95
110.94
110.93
110.91
110.90
110.87
110.85
102.76
102.73
102.72
102.69
102.63
102.60
102.59
102.56
77.42 cdcl3
77.16 cdcl3
76.91 cdcl3
F
F
S
S
F
F
B (dd)
142.16
A (dd)
145.44
D (dt)
102.66
C (ddd)
110.93
20
210
200
190
180
170
160
150
140
130
120
110
100
90
80
70
60
50
40
30
20
10
f1 (ppm)